

# Probing the Mid-level Vision Capabilities of Self-Supervised Learning

Xuwei Chen<sup>1</sup> Markus Marks<sup>2</sup> Zezhou Cheng<sup>1</sup>  
<sup>1</sup>University of Virginia <sup>2</sup>California Institute of Technology  
<https://midvision-probe.cs.virginia.edu/>

## Abstract

Mid-level vision capabilities — such as generic object localization and 3D geometric understanding — are not only fundamental to human vision but are also crucial for many real-world applications of computer vision. These abilities emerge with minimal supervision during the early stages of human visual development. Despite their significance, current self-supervised learning (SSL) approaches are primarily designed and evaluated for high-level recognition tasks, leaving their mid-level vision capabilities largely unexamined.

In this study, we introduce a suite of benchmark protocols to systematically assess mid-level vision capabilities and present a comprehensive, controlled evaluation of 22 prominent SSL models across 8 mid-level vision tasks. Our experiments reveal a weak correlation between mid-level and high-level task performance. We also identify several SSL methods with highly imbalanced performance across mid-level and high-level capabilities, as well as some that excel in both. Additionally, we investigate key factors contributing to mid-level vision performance, such as pretraining objectives and network architectures. Our study provides a holistic and timely view of what SSL models have learned, complementing existing research that primarily focuses on high-level vision tasks. We hope our findings guide future SSL research to benchmark models not only on high-level vision tasks but on mid-level as well.

## 1. Introduction

Mid-level vision capabilities [42] (Fig. 1a) play a vital role in human visual development and daily life activities. By the age of one, children can re-organize retinal images into objects (*i.e.*, *perceptual grouping*), construct the visual world in three dimensions (*i.e.*, *3D geometric understanding*), track moving objects (*i.e.*, *cross-view correspondence*), grasp and bite these objects without knowing their semantics, and purposefully navigate through the 3D world. Importantly, such mid-level perception is developed without supervision [33].

On the other hand, self-supervised learning (SSL) in

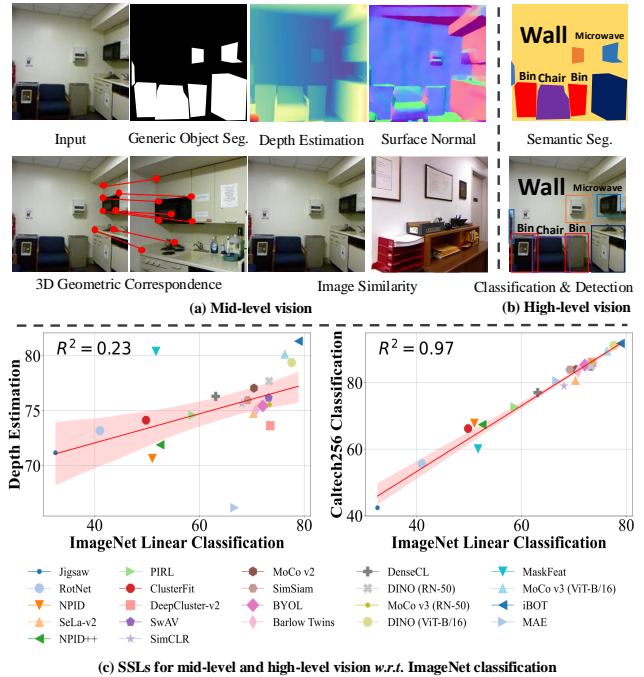


Figure 1. **Mid-Level Vision vs. High-Level Vision Tasks.** We provide a comprehensive evaluation of prominent self-supervised learning methods (SSLs) across a wide range of mid-level vision tasks (a), complementing the standard evaluation in high-level vision tasks (b). Although SSL performance in mid-level vision tasks (*e.g.*, depth estimation) is positively correlated with ImageNet linear probing (c, left), this correlation is much weaker than that observed among high-level vision tasks (*e.g.*, Caltech-256 [27] vs. ImageNet classification) (c, right), as indicated by the  $R^2$  statistics.

computer vision has made significant strides [5–8, 25, 43, 46, 47, 66, 71]. The goal of SSL is to learn visual representations from unlabeled data so that these pretrained representations can be applied to a wide range of downstream tasks, reducing the need for human annotations and enhancing learning efficiency and performance. However, SSL is predominantly evaluated based on performance in high-level visual recognition tasks, such as image classification, object detection, and semantic segmentation (Fig. 1b).

At the same time, the mid-level vision capabilities of SSL models are largely under-explored. To fill this gap, this paper addresses the following questions:

- *Does strong high-level vision performance of SSLs indicate strong mid-level vision capabilities?*
- *What makes an SSL model effective for mid-level vision tasks?*

To answer these questions, we comprehensively evaluate SSLs in a wide range of mid-level vision tasks, including generic object segmentation, monocular depth and surface normal estimation, geometric correspondence, and mid-level image similarity (Fig. 1a and Tab. 2). We then relate the mid-level vision performance of these SSLs to their high-level vision performance. Our evaluations covers 22 seminal SSL approaches (Tab. 1) from diverse categories developed in the past decades (*e.g.* pretext tasks [25, 46], contrastive learning [6, 7, 9, 28, 66], self-distillation [5], and generative modeling [31, 62]). To make a controlled study and fair comparisons across different SSLs, our study primarily focuses on SSLs with publicly available checkpoints pretrained on ImageNet1K [12]. This allows us to gain insights into what factors may contribute to the mid-level vision capabilities in SSL (*e.g.*, training objectives, network architectures, *etc.*).

Our observations are as follows:

- The mid-level vision capabilities of SSLs are positively correlated with high-level vision. However, that correlation is generally weaker than that among high-level vision tasks (Fig. 1c and Fig. 2).
- Some SSLs have highly imbalanced mid-level and high-level vision capabilities. For instance, MAE [32] underperforms most SSLs in the mid-level vision tasks while having competitive high-level vision performance; MaskFeat [62] has better mid-level performance than most SSLs with similar high-level vision (Fig. 5).
- Network architectures, model capacity, and pretraining strategies impact mid-level vision capabilities. In general, ViT [14] outperforms ResNet [29]; Increasing the network capacity is beneficial (Tab. 3); The leading methods are generally based on generative modeling (Fig. 5).

Our study is built upon Probe3D [17], a recent work that evaluates the 3D awareness of visual models. In this work, we explore a broader range of mid-level vision tasks. Furthermore, our study primarily focuses on SSLs pretrained exclusively on ImageNet1K, while Probe3D probes visual foundation models that are trained from very diverse training configurations such as varying supervision signals (*e.g.* CLIP [51]) and dataset sizes. Our controlled settings allow us to gain insights into the factors contributing to model performance. Our exploration is also closely related to prior works that benchmark SSLs in various vision tasks [18, 26, 45, 56], such as out-of-domain classification [41] and fine-grained recognition [55, 58]. Unlike

these works, our evaluation includes more recent SSLs, providing a timely study on this topic.

In summary, our study offers a comprehensive view of the representations learned by SSL models. We hope these findings inspire practical approaches that perform well across both mid-level and high-level vision tasks. We will release our benchmark suite to support future SSL benchmarking in the research community.

## 2. Related Work

**Self-Supervised Learning (SSL).** The goal of self-supervised learning (SSL) in computer vision is to pre-train image representations using unlabeled data, enabling these representations to be transferred effectively to various downstream tasks. Early SSL methods leveraged a range of pretext tasks, such as colorization [70], rotation prediction [25], jigsaw puzzle solving [46], and inpainting [48]. Recent advances have focused on contrastive learning [6, 7, 28, 30, 66, 69] and generative modeling [13, 32, 38, 49, 62]. Despite extensive research, SSL performance is primarily evaluated on high-level vision tasks (*e.g.*, ImageNet classification, object detection), overlooking the practical relevance of mid-level vision tasks. In this work, we focus on evaluating SSL methods on mid-level vision tasks.

**Self-Supervised Pretraining for 3D Vision.** Unlike most SSL methods focusing on 2D visual recognition tasks, a few recent works explore SSLs for 3D vision. For example, CroCo [63] adopts masked image modeling to learn 3D representations from image pairs showing the same scene from different viewpoints. Despite the improvement in downstream 3D vision tasks, CroCo compromises high-level recognition performance. As a followup, CroCo-v2 [64] extends the training data of CroCo to a large dataset of natural images and demonstrates improved performance in downstream optical flow and stereo vision tasks. However, learning representations for 3D vision tasks remains under-explored.

**Benchmarking Self-Supervised Learning.** Numerous studies underscore the growing importance of empirically evaluating general-purpose representation learning. For example, Goyal *et al.* [26] provide extensive benchmarking of SSLs across multiple downstream tasks, including classification, navigation, object detection, and surface normal estimation. Newell *et al.* [45] examine the effectiveness of SSLs under various configurations (*e.g.*, annotation quantities) in downstream tasks such as pose estimation and depth estimation. Ericsson *et al.* [18] evaluate 13 SSLs across 40 downstream vision tasks, demonstrating a weak correlation between SSL performance on ImageNet classification and tasks like few-shot learning, object detection, and dense prediction. More recently, Marks *et al.* [41] studied how classification-based SSL evaluation protocols cor-

relate with and predict downstream performance on out-of-domain datasets. In line with these works, we comprehensively evaluate existing SSLs across various downstream tasks. We focus on mid-level vision performance and how it relates to high-level vision.

**Benchmarking Visual Foundation Models.** More recently, several studies have evaluated large visual foundation models (VFMs) that are not exclusively trained by self-supervised learning methods (*e.g.*, CLIP [51]). For example, Probe3D [17] examines the 3D awareness of VFMs [5, 35], while Cambrian-1 [56] utilizes large language models (LLMs) and visual instruction tuning to assess visual representations across various 2D and 3D vision tasks. Since VFMs are typically trained with diverse approaches (*e.g.*, different supervision signals, datasets, and architectures), isolating the factors contributing to the performance of the representations they learn is challenging. In contrast, we conduct a controlled evaluation of SSL models that provide publicly available checkpoints pretrained on ImageNet1K. This approach enables fair comparisons across SSLs and offers deeper insights into their methodologies.

### 3. Background: Vision Task Taxonomy

There exist numerous computer vision tasks [68] which can be categorized from different perspectives. We briefly introduce two popular frameworks in this section:

- **Bottom-up Hierarchical Vision.** David Marr [42] proposes to break up the vision system into low-level, mid-level, and high-level stages. Low-level vision tasks aim to extract edges, contours, and blobs from raw pixels, while high-level vision concerns the semantics, functionality, and holistic 3D shape of objects. Mid-level vision, lying in-between the low-level and high-level vision, addresses the view-centric geometric properties of surfaces (*e.g.*, depth and surface normal), generic object segmentation and localization *without semantics*, cross-view image correspondences, and so on. This framework favors a feed-forward and bottom-up vision process.
- **Three R’s of Vision.** Malik *et al.* [40] categorize vision tasks into recognition, reconstruction, and reorganization. Recognition refers to the task of assigning semantic categories to images. Reconstruction concerns the estimation of 3D structures. Reorganization addresses the grouping and segmentation of images on spatial or perceptual similarity. Instead of a bottom-up process, 3R’s emphasizes the mutual benefits and relationship across these three visual capabilities.

Both frameworks highlight the importance of the non-semantic vision tasks — mid-level vision in Marr’s framework, reconstruction and reorganization in 3R’s. We adopt

the term “mid-level” for the convenience of differentiating from high-level recognition tasks. However, the underlying vision mechanism remains under debate.

### 4. Experimental Setup

In this section, we first introduce the SSLs considered in this work (Tab. 1) and our generic evaluation protocols for probing these SSLs. We then present the mid-level vision tasks in detail, including their definitions, datasets, and evaluation approaches (Sec. 4.1- 4.3 and Tab. 2).

Our probing approaches are largely inspired by Probe3D [17], the recent work that evaluates the 3D awareness of visual foundation models (VFMs). The VFMs are usually trained under distinct settings (*e.g.* supervision signals, dataset sizes, network architectures and capacity), while we aim at probing self-supervised visual models that are trained with similar configurations. Therefore, our work provides a complementary study, specifically a more controlled setting, compared to Probe3D [17].

**Self-Supervised Models.** Tab. 1 presents an overview of the SSL models considered in our study. We primarily focus on SSLs that have publicly available checkpoints pretrained on ImageNet1K [12], with standard neural network architectures (*e.g.* ResNet50 [29] or Vision Transformers (ViT) [14]) as the image feature extractor. These SSLs cover a wide range of pretraining strategies, including clustering, contrastive learning, generative modeling, or a mixture of different training objectives. Targeting a comprehensive benchmark, we track the SSL literature back to classic methods that learn image representations from pre-text tasks such as Jigsaw [46] and RotNet [25]. Our selection of SSLs is inspired by Marks *et al.* [41], which provides a detailed study of the evaluation protocols of SSLs.

**Generic Evaluation Protocols.** Many mid-level vision tasks can be formulated as dense prediction (*e.g.*, depth estimation). Unlike image classification, dense prediction requires local pixel or patch representations as input, and the main design choice is to decide which network layers (*e.g.*, ResNet layers or ViT blocks) to extract the dense features from. Following Probe3D, we use the DPT decoder [53], a non-linear dense multi-scale network. For ResNet [29], we use the outputs of the last four ResNet blocks as the input to the DPT head, following the architecture of the feature pyramid network [37]; For ViT [14], following Probe3D, the network is split into four blocks evenly, and the features are extracted after each block — for ViT-B, we extract features after layers 3, 6, 9, and 12. Like Probe3D, we probe the frozen representations to evaluate the capabilities of learned representations instead of their transferability. We provide task-specific evaluation protocols in the following sections and hyperparameter settings in the supplementary material.

ID	SSL	Architecture	Category
1	Jigsaw [46]	ResNet50	Pre-text
2	RotNet [25]	ResNet50	Pre-text
3	NPID [66]	ResNet50	Contrastive
4	NPID++ [43]	ResNet50	Contrastive
5	PIRL [43]	ResNet50	Contrastive
6	ClusterFit [67]	ResNet50	Clustering
7	SwAV [4]	ResNet50	Clustering
8	SeLa-v2 [4]	ResNet50	Clustering
9	DeepCluster-v2 [4]	ResNet50	Clustering
10	SimCLR [6]	ResNet50	Contrastive
11	MoCo-v2 [8]	ResNet50	Contrastive
12	SimSiam [7]	ResNet50	Contrastive
13	DenseCL [59]	ResNet50	Contrastive
14	BYOL [28]	ResNet50	Contrastive
15	Barlow Twins [69]	ResNet50	Contrastive
16	MoCo-v3 [9]	ResNet50	Contrastive
17	DINO [5]	ResNet50	Self-distillation
18	MoCo-v3 [9]	ViT-B/16	Contrastive
19	DINO [5]	ViT-B/16	Self-distillation
20	MAE [32]	ViT-B/16	Generative
21	iBOT [71]	ViT-B/16	Mixture
22	MaskFeat [62]	ViT-B/16	Generative

Table 1. **Evaluated Self-Supervised Learning Methods (SSLs).** We provide a comprehensive evaluation of SSLs that provide publicly available checkpoints trained from the ImageNet1K dataset [12]. We categorize SSLs based on their training objectives and network backbones. *Mixture* denotes the combination of different SSLs (e.g., iBOT [71]). The SSLs are listed in order of their publication year.

#### 4.1. Generic Object Segmentation

Generic object segmentation (or figure-ground segmentation) refers to the task of separating objects (figure) from the surrounding background *without any semantics*. This mid-level vision task is different from semantic segmentation (*i.e.*, assigning each pixel to a *semantic category*) which is commonly used for evaluating the high-level visual capabilities of SSLs.

We use the VOC07 and VOC12 datasets [19, 20] as our benchmarks, following prior research on unsupervised object segmentation [57, 60, 61]. Given a pretrained feature extractor, we freeze the backbone and train a DPT decoder [52] with a simple binary cross-entropy loss (BCE). We use standard segmentation metrics (e.g., mean IoU) to measure the performance of SSLs in this task.

#### 4.2. Monocular Surface Reconstruction

We evaluate SSLs in two tasks related to monocular 2.5D surface reconstruction: depth and surface normal estimation from Probe3D [17]. Even though these two tasks are closely related, they rely on different visual cues and cap-

ture distinct geometric properties.

We evaluate depth estimation and surface normal prediction at both scene and object levels. For scene-level performance, we employ the NYUv2 dataset [44], a widely used benchmark for indoor environments. Object-level depth is assessed using the NAVI dataset [34], which provides diverse object instances across scenes and orientations.

We present the task-specific configurations as follows.

**Monocular Depth Estimation** The task aims at predicting pixel-wise depth from monocular images. We adopt the formulation of binned depth estimation from AdaBins [21], instead of the classical regression approaches [15]. We estimate the scale-invariant depth for object-centric images (e.g., NAVI) while predict metric depths on scene-centric datasets (e.g., NYUv2). We report root-mean-squared error (RMSE) and recall at various threshold ratios.

**Surface Normal Estimation.** This task is to predict per-pixel surface direction. We train the DPT head with the uncertainty-aware angular loss [2]. As for depth estimation, we report RMSE and percentage recall at various angular thresholds.

#### 4.3. Multiview Correspondence

In this section, we consider the tasks of estimating correspondences across multiple views that involve mid-level variations, such as changes in camera perspective and object motion. These mid-level variations differ from low-level variations in image properties (e.g., color and texture) and high-level variations in semantic attributes (e.g., object categories). Specifically, we probe SSLs in two tasks: geometric correspondence and mid-level image similarity. Following Probe3D [17], we extract image or pixel representations from pretrained SSLs model without additional training.

**Geometric Correspondence** This task aims to build pixel correspondences across two views that depict the same 3D scene. Our evaluation follows Probe3D [17]. Specifically, we estimate the pixel correspondences using the dense feature maps extracted from pretrained SSL models. We use the Paired ScanNet [10] to evaluate scene-centric images and the NAVI dataset [34] for object-centric images. We sample views with a maximum rotation of 120 degrees to ensure that a mutually visible surface exists without a large viewpoint change. We report the correspondence recall — the percentage of correspondence that falls within some defined distance.

**Mid-Level Image Similarity** The task aims at measuring the similarity of two images with mid-level variations (e.g., viewpoint). We evaluate the SSLs on the NIGHTS dataset collected by DreamSim [23]. Specifically, for each triplets  $(x, \tilde{x}_0, \tilde{x}_1)$  from the NIGHTS dataset, we predict whether  $\tilde{x}_0$  or  $\tilde{x}_1$  is more similar to the reference image  $x$ . We denote a distance between two images as  $D(x, \tilde{x}; f_\theta) =$



Hierarchy	Tasks	Type	Benchmarks	Losses	Metrics
High-level	Image Classification	2D	ImageNet1K [54]	CE	Accuracy
	Object Detection	2D	VOC07 [19], COCO [36]	CE+L2	AP
	Semantic Segmentation	2D	COCO [36]	CE	mIOU
Mid-level	Generic Object Segmentation	2D	VOC07 [19], VOC12 [20]	BCE	F1, mIoU, Acc
	Depth Prediction	3D	NAVI [34], NYU [44]	AdaBin	RMSE, $\epsilon_1$ , $\epsilon_2$ , $\epsilon_3$
	Surface Normal Estimation	3D	NAVI [34], NYU [44]	Angular	RMSE, $\epsilon_1$ , $\epsilon_2$ , $\epsilon_3$
	Geometric Correspondence	3D	NAVI [34], ScanNet [11]	Training-free	2D, 3D Recall
	Mid-level Image Similarity	2D	NIGHTS [24]	Training-free	Retrieval Score (F1-Score)

Table 2. **Probing Tasks.** In comparison with the standard SSL evaluation protocols that primarily focus on high-level vision tasks (**top**), we provide a comprehensive, systematic, and controlled evaluation of SSL in mid-level vision tasks (**bottom**). Our evaluations cover 2D and 3D vision with a wide range of benchmarks. The  $\epsilon_1$ ,  $\epsilon_2$  and  $\epsilon_3$  in depth and surface normal estimation represents recall at different threshold ratios [16, 22]. Detailed descriptions of each metric can be found in the supplementary.

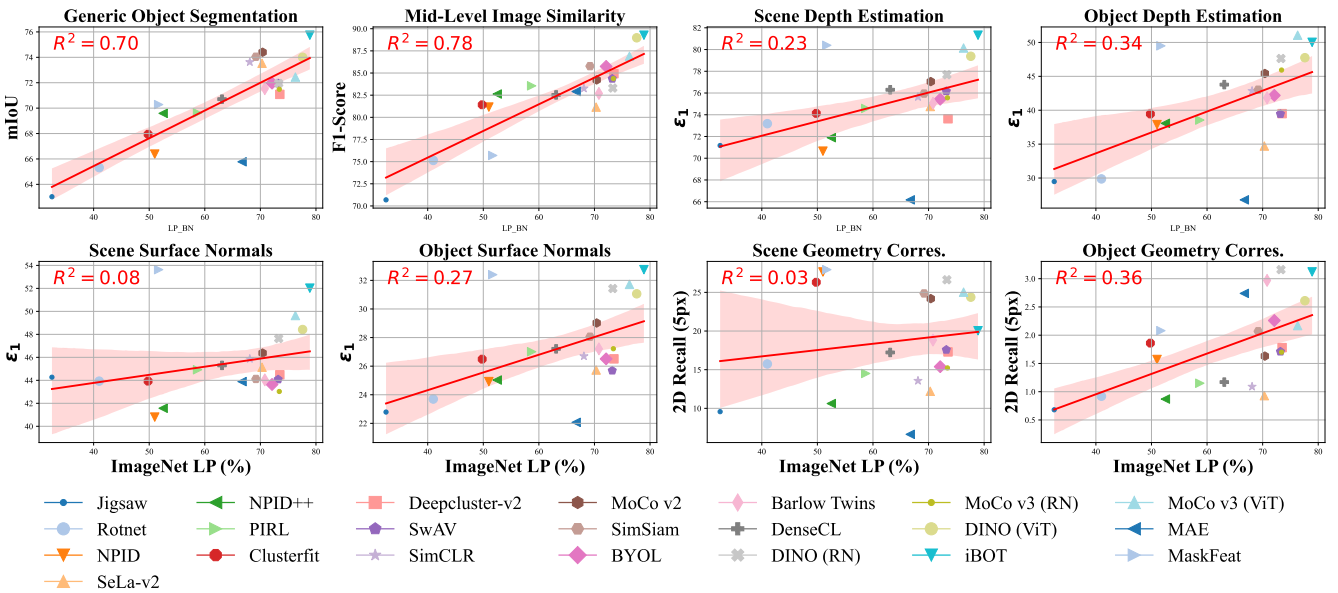


Figure 2. **Mid-Level Vision v.s. ImageNet Linear Probing.** We report the performance of self-supervised learning methods on mid-level vision tasks (y-axis) against their ImageNet 1K linear classification accuracy. Metrics are detailed in Tab. 2. Linear regression shows correlation with  $R^2$  in each plot’s top-left corner, and the red shaded area marks the 95% confidence interval.

$1 - \cos(f_\theta(x), f_\theta(\tilde{x}))$  where  $f_\theta$  is the image representations from pretrained SSLs. For ViT, we use the CLS tokens taken from the last layer; For ResNet, we use the global image representation in the output layer. The model’s vote is calculated as follows: if  $d_1 < d_0$ , then  $\hat{y} = 1$ ; otherwise, if  $d_0 < d_1$ , then  $\hat{y} = 0$ , where  $d_0 = D(x, \tilde{x}_0; f_\theta)$  and  $d_1 = D(x, \tilde{x}_1; f_\theta)$ . We use voting accuracy as our evaluation metric.

## 5. Analysis

### 5.1. Does strong high-level performance imply strong mid-level performance?

**Yes, to some extent.** As ImageNet (IN1k) probing results improve, we generally observe a corresponding enhance-

ment in mid-level vision tasks, as depicted in Fig. 2. This positive trend indicates that SSL models capable of high-level visual recognition tend to provide better representations for mid-level vision tasks as well, benefiting tasks that leverage spatial and structural information.

### Some mid-level tasks are highly correlated with high-level.

A per-task closer examination, however, reveals nuances in this relationship. For example, *generic object segmentation* shows the highest correlation with high-level tasks, achieving a coefficient of determination ( $R^2 = 0.70$ ). This suggests that high-level features indeed capture spatial structures that enhance segmentation accuracy. Mid-level and high-level vision also correlate highly in the task of *mid-level image similarity*. This indicates that the high-

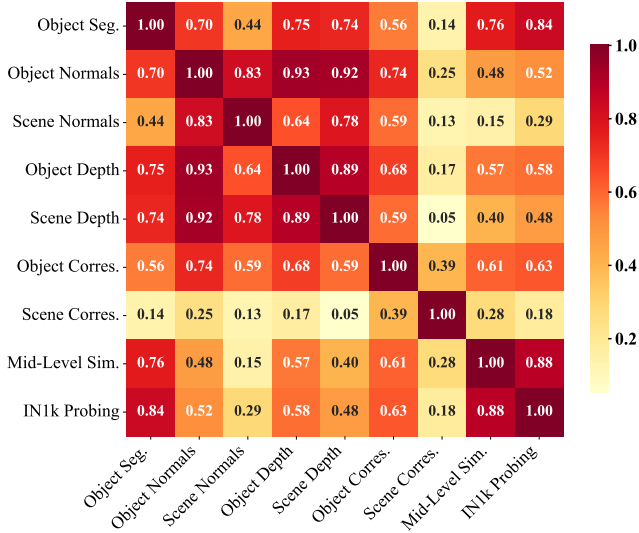


Figure 3. **Cross-task performance correlation.** We present Pearson coefficients across mid-level and high-level vision tasks. We use the same set of metrics we used in Fig. 2.

level image representations are invariant to mid-level variations to some extent (e.g., viewpoint variations).

**3D geometric understanding is weakly correlated with high-level vision.** For tasks like *scene surface normal estimating*, we observe notably weaker correlations. These tasks often require intricate, fine-grained geometric and surface features that high-level SSL objectives alone do not sufficiently capture. This gap implies that mid-level vision depends on specialized cues not fully addressed by high-level feature extraction.

**Correlation across mid-level vision tasks.** Fig. 3 shows the Pearson correlations across tasks. We find a strong correlation between object segmentation and mid-level image similarity (coefficients above 0.76). Object segmentation further correlates well with depth estimation and object-level multi-view geometric correspondence, indicating that spatial understanding aids segmentation and underscores the importance of 3D awareness in image understanding. In contrast, scene geometry correspondence correlates weaker with other mid-level and high-level tasks. Mid-level image similarity aligns with object segmentation and correspondence but correlates less with 3D tasks.

**Ranking in mid-level vision.** In Fig. 5, we present a comparative ranking of SSL models based on their performance across mid-level vision tasks and ImageNet probing. Each model received a task-specific rank, and we computed an average score, with higher scores indicating stronger performance in both mid-level and high-level vision tasks. Our analysis suggests an imbalance in model performance, with

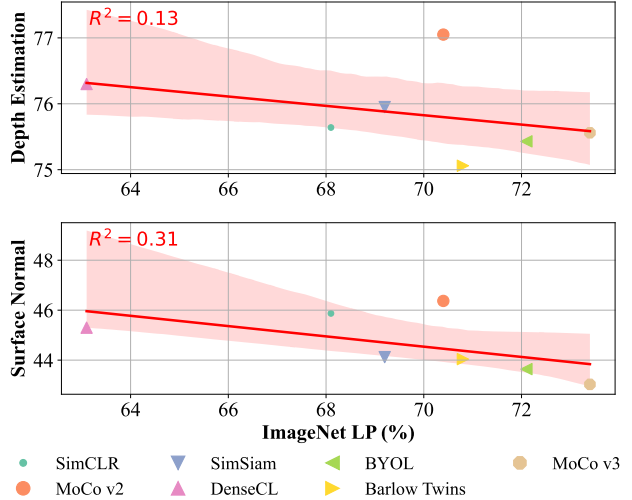


Figure 4. **Mid-Level Vision v.s. ImageNet Linear Probing with Contrastive Learning Methods.** We examine several contrastive learning methods [6–9, 28, 59, 69] and observe a negative correlation between ImageNet linear probing accuracy and task performance. Depth estimation results are shown at the top, with surface normal estimation results at the bottom. The y-axis represents prediction accuracy, where higher values indicate better performance.

some models excelling in high-level tasks but showing comparatively modest capabilities in mid-level vision tasks. Notably, MaskFeat stands out as an exception, demonstrating a significant advantage in mid-level vision tasks over high-level performance.

Conversely, MAE ranks lower on mid-level tasks, demonstrating limited proficiency in capturing finer visual details. In the following sections, we will discuss the specifics of MAE and MaskFeat.

Notably, iBOT [71] and DINO [4] rank among the top performers, exhibiting strong capabilities in both mid-level and high-level vision tasks. In contrast, pretext pre-trained models like RotNet [25] and Jigsaw [46] fall behind other SSL methods.

## 5.2. What makes a strong mid-level vision model?

**Training objective.** We observe that the top-performing SSL models in mid-level vision tasks are typically generative-based, such as iBOT [71] and MaskFeat [62]. In contrast, recent contrastive self-supervised learning (SSL) models [6–9, 28, 59, 69] show an inverse relationship between mid-level vision performance and ImageNet linear probing accuracy, as illustrated in Fig. 4.

Although these methods have improved ImageNet linear probing accuracy by over 10%, they exhibit notable declines in mid-level vision tasks. We illustrate this trend with model performance on depth and surface normal estimation and provide a broader analysis across six additional tasks in the

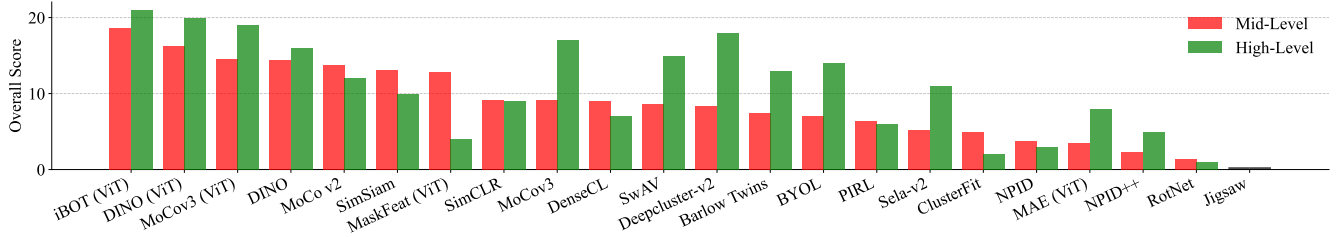


Figure 5. **Ranking SSLs based on Overall Score.** Comparative ranking of SSL models based on performance in mid-level vision tasks and ImageNet probing. Models are ranked per task, and average scores reflect overall performance across mid-level and high-level vision tasks, with higher scores indicating stronger results.

supplementary materials. Notably, SSL models pre-trained on pretext tasks show the lowest performance on mid-level vision tasks.

**Network architecture.** We further compare ViT-B (ViT Base) and ViT-L (ViT Large) backbones with the same SSL method in Tab. 3. Our findings show that ViT-L models tend to perform better than ViT-B across mid-level vision tasks. In particular, we evaluate two popular SSL models, iBOT and MAE, on both ViT-B and ViT-L backbones. This pattern suggests that larger backbones like ViT-L may capture mid-level vision features better.

**Network capability.** We also compare ViT-B and ViT-L backbones using the same SSL method in Tab. 3. Our results indicate that ViT-Large models generally achieve higher scores across various mid-level vision tasks. Specifically, we examine two popular SSL models, iBOT and MAE, with ViT-B and ViT-L backbones. This trend suggests that larger models are better at capturing mid-level vision features.

### 5.3. Which SSL works the best per task?

In Tab. 4, we highlight the best-performing models for each task. iBOT [71] consistently leads in most mid-level vision tasks while MaskFeat performs even better on scene correspondence and scene surface normal. DINO works the best on object correspondence and achieves quite competitive results compared to other SSLs.

### 5.4. Analysis of specific SSL

**MAE.** MAE [31] stands out as a clear outlier, as illustrated in Fig. 2 and Fig. 5. MAE consistently performs poorly on mid-level vision tasks compared to other ViT-based SSLs such as iBOT [71] and MaskFeat [62].

**MaskFeat.** In Fig. 2 and Fig. 5, we observe that MaskFeat [62] demonstrates surprisingly strong mid-level vision capabilities despite showing relatively modest performance in high-level vision tasks. Since the MaskFeat checkpoint we used was trained exclusively on the ImageNet-1K

dataset and followed a training process similar to MAE, we attribute its mid-level vision strength to its choice of target features. Unlike models trained on raw pixels, tokens, or high-level features, MaskFeat is optimized on HOG (Histograms of Oriented Gradients) features, which are widely used for keypoint detection in methods such as SIFT [39]. Importantly, HOG does not rely on any external models, making it a robust feature for capturing mid-level vision attributes. This finding suggests that incorporating mid-level vision-relevant features, like HOG, into SSL training may enhance model performance on mid-level vision tasks.

**SSLs based on pre-text tasks.** RotNet and Jigsaw are the two lowest-performing SSLs on mid- and high-level vision. Given that they are the early design of SSLs, it re-validate our claim that ImageNet (IN1k) probing results improve, we generally observe a corresponding enhancement in mid-level vision task performance.

### 5.5. How do visual foundation models (VFMs) perform?

Even though our study aims to conduct a controlled benchmarking of SSLs in the mid-level vision tasks, we put VFMs into our context in this section to understand the comparison between the latest visual foundation models and the set of SSLs we analyzed. We observed that CLIP is much worse than most of the SSLs. DINO-v2 is the winner. We include a comparison in Fig. 6 focusing on depth estimation capability. We include this comparison across more tasks in the appendix.

**DINO-V2** [47]. Our findings, consistent with Probe3D and Cambrian-1 [56], show DINO-V2 as the best-performing model across both ImageNet linear probing and mid-level vision tasks, making it a standout choice for comprehensive vision capabilities.

**CLIP** [51]. CLIP’s overall performance is notably lower across mid-level tasks, as reported in Probe3D [17] and Cambrian-1 [56]. This suggests that, while generalizable for 2D understanding, CLIP may be less suited for tasks requiring 3D spatial understanding.

SSLs	Backbone	Object Seg.	Object SNorm.	Scene SNorm.	Object Depth	Scene Depth	Object Corres.	Scene Corres.	Image Sim.
MoCo-v3 [9]	RN-50	71.48	27.22	43.03	45.93	75.56	1.7	15.23	84.37
MoCo-v3 [9]	ViT-B/16	<b>72.45</b>	<b>31.72</b>	<b>49.64</b>	<b>51.07</b>	<b>80.14</b>	<b>3.12</b>	<b>25.03</b>	<b>86.90</b>
DINO [5]	RN-50	71.95	<b>31.43</b>	47.64	47.63	77.68	<b>3.16</b>	<b>26.63</b>	83.31
DINO [5]	ViT-B/16	<b>74.00</b>	31.06	<b>48.42</b>	<b>47.75</b>	<b>79.38</b>	2.61	24.38	<b>89.36</b>

SSLs	Model Size	Object Seg.	Object Norm.	Scene Norm.	Object Depth	Scene Depth	Object Corres.	Scene Corres.	Image Sim.
iBOT	B/16	<b>75.74</b>	32.75	52.02	50.02	81.32	3.12	<b>20.04</b>	<b>89.27</b>
iBOT	L/16	75.32	<b>35.65</b>	<b>54.53</b>	<b>52.56</b>	<b>85.14</b>	<b>3.16</b>	14.79	82.37
MAE	B/16	65.77	22.67	43.89	26.78	66.17	2.74	6.64	82.91
MAE	L/16	<b>66.58</b>	<b>26.60</b>	<b>45.60</b>	<b>26.81</b>	<b>70.22</b>	<b>2.93</b>	<b>10.05</b>	<b>84.26</b>

Table 3. **Impact of Network Architecture and Model Size on Mid-Level Vision Performance.** The top table demonstrates that the Vision Transformer (ViT) [14] generally outperforms ResNet-50 (RN-50) [29] across most mid-level vision tasks when using MoCo-v3 or DINO as the self-supervised pretraining method. The bottom table shows that larger model sizes tend to enhance mid-level vision capabilities. Detailed numerical comparisons are provided in the supplementary material.

Model	Image Sim.	Object Corres.	Object Depth	Object SNorm.
DINO (RN-50)	83.31	<b>3.16</b>	47.63	31.43
MaskFeat [62]	75.70	2.08	<u>49.50</u>	<u>32.40</u>
MoCo v3	<u>84.37</u>	1.70	45.93	27.22
iBOT [71]	<b>89.27</b>	<u>3.12</u>	<b>50.02</b>	<b>32.75</b>

Model	Object Seg.	Scene Corres.	Scene Depth	Scene SNorm.
DINO (RN-50)	71.95	<u>26.63</u>	77.68	47.64
MaskFeat [62]	70.28	<b>27.94</b>	<u>80.39</u>	<b>53.63</b>
MoCo v3	71.48	15.23	75.56	43.03
iBOT [71]	<b>75.74</b>	20.04	<b>81.32</b>	<u>52.02</u>

Table 4. **Top SSL Methods in Mid-Level Vision Tasks.** iBOT outperformed all other SSL methods (listed in Tab. 1) in multiple mid-level vision tasks. Surprisingly, despite the low performance on ImageNet linear classification, MaskFeat achieved leading results in depth and surface normal estimation.

**CroCo** [65]. Using depth estimation as a representative task, we observe that CroCo performs competitively in mid-level vision tasks despite lagging in high-level vision tasks. Pretrained on synthetic multi-view image datasets, CroCo learns strong 3D-aware image representations. This distinction underscores its potential for 3D-specific applications, where spatial understanding is prioritized over high-level visual semantics because of its design choice.

## 6. Discussion

In conclusion, this study introduces a suite of benchmark protocols to systematically evaluate mid-level vision capabilities, offering a comprehensive and controlled assessment of 22 SSL models across mid-level vision tasks. Our findings indicate a positive correlation between SSL performance in mid-level and high-level vision tasks, though this correlation is generally weaker than that observed within high-level tasks.

Some SSL models exhibit imbalanced performance across these task levels. For instance, MAE [32] underperforms in mid-level tasks despite competitive high-level per-

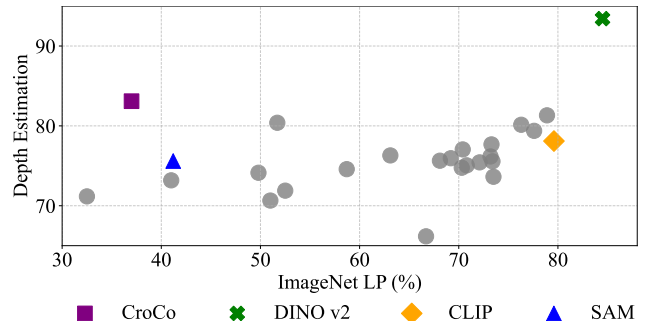


Figure 6. Comparison of ImageNet1K-Pretrained SSLs with models trained with larger datasets (*e.g.*, DINO-v2 [47]) or different training supervisions (*e.g.*, CLIP [51]) in the scene depth estimation task.

formance, while MaskFeat [62] excels in mid-level tasks relative to its high-level results (Fig. 5). Mid-level vision capabilities are influenced by factors such as network architecture, dataset size, and pretraining strategy. Overall, ViT [14] outperforms ResNet [29], increasing model capacity proves beneficial (Tab. 3), and generative modeling approaches often lead in performance (Fig. 5). Additionally, we compare SSL models with VFMs, finding that DINOv2 [47] leads in both mid-level and high-level vision tasks and language objectives (*e.g.*, CLIP) do not help on mid-level tasks.

Since SSL’s overall goal is to produce a very general feature representation that works well for a wide range of downstream tasks, we encourage the community to evaluate new SSL methods on both high- and mid-level tasks.

This work is limited by resources, which prevents us from scaling up our experiments to more tasks and models, and we did not include ending tasks such as navigation and robotic manipulation to emphasize mid-level vision’s role further. We provide details of our probing hyper-parameters and include visualizations for each task in the supplementary materials.



## 7. Acknowledgement

The authors gratefully acknowledge Research Computing at the University of Virginia for providing the computational resources and technical support that made the results in this work possible. [Research Computing at UVA](#).

## References

- [1] Yuki Markus Asano, Christian Rupprecht, and Andrea Vedaldi. Self-labelling via simultaneous clustering and representation learning, 2020. [2](#)
- [2] Gwangbin Bae, Ignas Budvytis, and Roberto Cipolla. Estimating and exploiting the aleatoric uncertainty in surface normal estimation, 2021. [4](#)
- [3] Mathilde Caron, Piotr Bojanowski, Armand Joulin, and Matthijs Douze. Deep clustering for unsupervised learning of visual features, 2019. [3](#)
- [4] Mathilde Caron, Ishan Misra, Julien Mairal, Priya Goyal, Piotr Bojanowski, and Armand Joulin. Unsupervised learning of visual features by contrasting cluster assignments, 2021. [4](#), [6](#), [2](#), [3](#), [8](#), [9](#), [10](#)
- [5] Mathilde Caron, Hugo Touvron, Ishan Misra, Hervé Jégou, Julien Mairal, Piotr Bojanowski, and Armand Joulin. Emerging properties in self-supervised vision transformers. In *ICCV*, 2021. [1](#), [2](#), [3](#), [4](#), [8](#), [9](#), [10](#)
- [6] Ting Chen, Simon Kornblith, Mohammad Norouzi, and Geoffrey Hinton. A simple framework for contrastive learning of visual representations. *ICML*, 2020. [2](#), [4](#), [6](#), [1](#), [8](#), [9](#), [10](#)
- [7] Xinlei Chen and Kaiming He. Exploring simple siamese representation learning. In *CVPR*, 2021. [2](#), [4](#), [8](#), [9](#), [10](#)
- [8] Xinlei Chen, Haoqi Fan, Ross Girshick, and Kaiming He. Improved baselines with momentum contrastive learning. *arXiv preprint arXiv:2003.04297*, 2020. [1](#), [4](#), [2](#), [8](#), [9](#), [10](#)
- [9] Xinlei Chen, Saining Xie, and Kaiming He. An empirical study of training self-supervised vision transformers, 2021. [2](#), [4](#), [6](#), [8](#), [3](#), [9](#), [10](#)
- [10] Angela Dai, Angel X Chang, Manolis Savva, Maciej Halber, Thomas Funkhouser, and Matthias Nießner. Scannet: Richly-annotated 3d reconstructions of indoor scenes. In *CVPR*, 2017. [4](#)
- [11] Angela Dai, Angel X. Chang, Manolis Savva, Maciej Halber, Thomas Funkhouser, and Matthias Nießner. Scannet: Richly-annotated 3d reconstructions of indoor scenes, 2017. [5](#)
- [12] Jia Deng, Wei Dong, Richard Socher, Li-Jia Li, Kai Li, and Li Fei-Fei. Imagenet: A large-scale hierarchical image database. In *CVPR*, 2009. [2](#), [3](#), [4](#), [1](#)
- [13] Xiaoyi Dong, Jianmin Bao, Yinglin Zheng, Ting Zhang, Dongdong Chen, Hao Yang, Ming Zeng, Weiming Zhang, Lu Yuan, Dong Chen, Fang Wen, and Nenghai Yu. Maskclip: Masked self-distillation advances contrastive language-image pretraining, 2023. [2](#)
- [14] Alexey Dosovitskiy. An image is worth 16x16 words: Transformers for image recognition at scale. *arXiv preprint arXiv:2010.11929*, 2020. [2](#), [3](#), [8](#)
- [15] David Eigen, Christian Puhrsch, and Rob Fergus. Depth map prediction from a single image using a multi-scale deep network. In *Neural Information Processing Systems*, 2014. [4](#)
- [16] David Eigen, Christian Puhrsch, and Rob Fergus. Depth map prediction from a single image using a multi-scale deep network, 2014. [5](#), [4](#)
- [17] Mohamed El Banani, Amit Raj, Kevis-Kokitsi Maninis, Abhishek Kar, Yuanzhen Li, Michael Rubinstein, Deqing Sun, Leonidas Guibas, Justin Johnson, and Varun Jampani. Probing the 3d awareness of visual foundation models. In *CVPR*, 2024. [2](#), [3](#), [4](#), [7](#)
- [18] Linus Ericsson, Henry Gouk, and Timothy M. Hospedales. How Well Do Self-Supervised Models Transfer? In *CVPR*, 2021. [2](#)
- [19] M. Everingham, L. Van Gool, C. K. I. Williams, J. Winn, and A. Zisserman. The PASCAL Visual Object Classes Challenge 2007 (VOC2007) Results. <http://www.pascal-network.org/challenges/VOC/voc2007/workshop/index.html>. [4](#), [5](#), [8](#)
- [20] M. Everingham, L. Van Gool, C. K. I. Williams, J. Winn, and A. Zisserman. The PASCAL Visual Object Classes Challenge 2012 (VOC2012) Results. <http://www.pascal-network.org/challenges/VOC/voc2012/workshop/index.html>. [4](#), [5](#), [8](#)
- [21] Shariq Farooq Bhat, Ibraheem Alhashim, and Peter Wonka. Adabins: Depth estimation using adaptive bins. In *2021 IEEE/CVF Conference on Computer Vision and Pattern Recognition (CVPR)*. IEEE, 2021. [4](#)
- [22] David F. Fouhey, Wajahat Hussain, Abhinav Gupta, and Martial Hebert. Single image 3d without a single 3d image. In *2015 IEEE International Conference on Computer Vision (ICCV)*, pages 1053–1061, 2015. [5](#), [4](#)
- [23] Stephanie Fu, Netanel Tamir, Shobhita Sundaram, Lucy Chai, Richard Zhang, Tali Dekel, and Phillip Isola. Dreamsim: Learning new dimensions of human visual similarity using synthetic data, 2023. [4](#)
- [24] Stephanie Fu, Netanel Tamir, Shobhita Sundaram, Lucy Chai, Richard Zhang, Tali Dekel, and Phillip Isola. Dreamsim: Learning new dimensions of human visual similarity using synthetic data. *Advances in Neural Information Processing Systems*, 36, 2024. [5](#)
- [25] Spyros Gidaris, Praveer Singh, and Nikos Komodakis. Unsupervised representation learning by predicting image rotations. In *ICLR*, 2018. [1](#), [2](#), [3](#), [4](#), [6](#), [8](#), [9](#), [10](#)
- [26] Priya Goyal, Dhruv Mahajan, Abhinav Gupta, and Ishan Misra. Scaling and benchmarking self-supervised visual representation learning. In *Proceedings of the IEEE/CVF International Conference on computer vision*, pages 6391–6400, 2019. [2](#)
- [27] Gregory Griffin, Alex Holub, and Pietro Perona. Caltech-256 object category dataset. 2007. [1](#)
- [28] Jean-Bastien Grill, Florian Strub, Florent Altché, Corentin Tallec, Pierre H. Richemond, Elena Buchatskaya, Carl Doherty, Bernardo Avila Pires, Zhaohan Daniel Guo, Mohammad Gheshlaghi Azar, Bilal Piot, Koray Kavukcuoglu, Rémi Munos, and Michal Valko. Bootstrap your own latent: A new approach to self-supervised learning, 2020. [2](#), [4](#), [6](#), [3](#), [8](#), [9](#), [10](#)

- [29] Kaiming He, Xiangyu Zhang, Shaoqing Ren, and Jian Sun. Deep residual learning for image recognition. In *CVPR*, 2016. 2, 3, 8
- [30] Kaiming He, Haoqi Fan, Yuxin Wu, Saining Xie, and Ross Girshick. Momentum contrast for unsupervised visual representation learning. In *CVPR*, 2020. 2
- [31] Kaiming He, Xinlei Chen, Saining Xie, Yanghao Li, Piotr Dollár, and Ross Girshick. Masked autoencoders are scalable vision learners, 2021. 2, 7, 3, 8, 9, 10
- [32] Kaiming He, Xinlei Chen, Saining Xie, Yanghao Li, Piotr Dollár, and Ross Girshick. Masked autoencoders are scalable vision learners. In *CVPR*, 2022. 2, 4, 8, 9, 10
- [33] Donald D Hoffman. *Visual intelligence: How we create what we see*. WW Norton & Company, 2000. 1
- [34] Varun Jampani, Kevis-Kokitsi Maninis, Andreas Engelhardt, Arjun Karapur, Karen Truong, Kyle Sargent, Stefan Popov, Andre Araujo, Ricardo Martin-Brualla, Kaushal Patel, Daniel Vlasic, Vittorio Ferrari, Ameesh Makadia, Ce Liu, Yuanzhen Li, and Howard Zhou. Navi: Category-agnostic image collections with high-quality 3d shape and pose annotations. In *NeurIPS*, 2023. 4, 5
- [35] Alexander Kirillov, Eric Mintun, Nikhila Ravi, Hanzi Mao, Chloe Rolland, Laura Gustafson, Tete Xiao, Spencer Whitehead, Alexander C Berg, Wan-Yen Lo, et al. Segment anything. In *ICCV*, 2023. 3
- [36] Tsung-Yi Lin, Michael Maire, Serge J. Belongie, Lubomir D. Bourdev, Ross B. Girshick, James Hays, Pietro Perona, Deva Ramanan, Piotr Dollár, and C. Lawrence Zitnick. Microsoft COCO: common objects in context. *CoRR*, abs/1405.0312, 2014. 5
- [37] Tsung-Yi Lin, Piotr Dollár, Ross Girshick, Kaiming He, Bharath Hariharan, and Serge Belongie. Feature pyramid networks for object detection. In *Proceedings of the IEEE conference on computer vision and pattern recognition*, pages 2117–2125, 2017. 3
- [38] Yuan Liu, Songyang Zhang, Jiacheng Chen, Kai Chen, and Dahua Lin. Pixmim: Rethinking pixel reconstruction in masked image modeling, 2023. 2
- [39] David G. Lowe. Distinctive image features from scale-invariant keypoints. *Int. J. Comput. Vision*, 60(2):91–110, 2004. 7
- [40] Jitendra Malik, Pablo Arbeláez, Joao Carreira, Katerina Fragkiadaki, Ross Girshick, Georgia Gkioxari, Saurabh Gupta, Bharath Hariharan, Abhishek Kar, and Shubham Tulsiani. The three r’s of computer vision: Recognition, reconstruction and reorganization. *Pattern Recognition Letters*, 72:4–14, 2016. 3
- [41] Markus Marks, Manuel Knott, Neehar Kondapaneni, Elijah Cole, Thijs Defraeye, Fernando Perez-Cruz, and Pietro Perona. A closer look at benchmarking self-supervised pre-training with image classification. *arXiv preprint arXiv:2407.12210*, 2024. 2, 3
- [42] David Marr. *Vision: A computational investigation into the human representation and processing of visual information*. MIT press, 2010. 1, 3
- [43] Ishan Misra and Laurens van der Maaten. Self-supervised learning of pretext-invariant representations. In *CVPR*, 2020. 1, 4, 2, 8, 9, 10
- [44] Pushmeet Kohli Nathan Silberman, Derek Hoiem and Rob Fergus. Indoor segmentation and support inference from rgb-d images. In *ECCV*, 2012. 4, 5
- [45] Alejandro Newell and Jia Deng. How useful is self-supervised pretraining for visual tasks? In *Proceedings of the IEEE/CVF Conference on Computer Vision and Pattern Recognition (CVPR)*, 2020. 2
- [46] Mehdi Noroozi and Paolo Favaro. Unsupervised learning of visual representations by solving jigsaw puzzles. In *ECCV*, 2016. 1, 2, 3, 4, 6, 8, 9, 10
- [47] Maxime Oquab, Timothée Darcet, Theo Moutakanni, Huy V. Vo, Marc Szafraniec, Vasil Khalidov, Pierre Fernandez, Daniel Haziza, Francisco Massa, Alaaeldin El-Nouby, Russell Howes, Po-Yao Huang, Hu Xu, Vasu Sharma, Shang-Wen Li, Wojciech Galuba, Mike Rabbat, Mido Assran, Nicolas Ballas, Gabriel Synnaeve, Ishan Misra, Herve Jegou, Julien Mairal, Patrick Labatut, Armand Joulin, and Piotr Bojanowski. Dinov2: Learning robust visual features without supervision, 2023. 1, 7, 8
- [48] Deepak Pathak, Philipp Krahenbuhl, Jeff Donahue, Trevor Darrell, and Alexei A Efros. Context encoders: Feature learning by inpainting. In *CVPR*, 2016. 2
- [49] Zhiliang Peng, Li Dong, Hangbo Bao, Qixiang Ye, and Furu Wei. Beit v2: Masked image modeling with vector-quantized visual tokenizers, 2022. 2, 3
- [50] Luigi Piccinelli, Christos Sakaridis, and Fisher Yu. idisc: Internal discretization for monocular depth estimation. In *CVPR*, 2023. 4
- [51] Alec Radford, Jong Wook Kim, Chris Hallacy, Aditya Ramesh, Gabriel Goh, Sandhini Agarwal, Girish Sastry, Amanda Askell, Pamela Mishkin, Jack Clark, et al. Learning transferable visual models from natural language supervision. In *International conference on machine learning*. PMLR, 2021. 2, 3, 7, 8
- [52] René Ranftl, Alexey Bochkovskiy, and Vladlen Koltun. Vision transformers for dense prediction. In *ICCV*, 2021. 4
- [53] René Ranftl, Alexey Bochkovskiy, and Vladlen Koltun. Vision transformers for dense prediction. In *Proceedings of the IEEE/CVF international conference on computer vision*, pages 12179–12188, 2021. 3
- [54] Olga Russakovsky, Jia Deng, Hao Su, Jonathan Krause, Sanjeev Satheesh, Sean Ma, Zhiheng Huang, Andrej Karpathy, Aditya Khosla, Michael Bernstein, Alexander C. Berg, and Li Fei-Fei. ImageNet Large Scale Visual Recognition Challenge. *International Journal of Computer Vision (IJCV)*, 115(3):211–252, 2015. 5, 1
- [55] Jong-Chyi Su, Zezhou Cheng, and Subhransu Maji. A Realistic Evaluation of Semi-supervised Learning for Fine-grained Classification. In *CVPR*, 2021. 2
- [56] Shengbang Tong, Ellis Brown, Penghao Wu, Sanghyun Woo, Manoj Middepogu, Sai Charitha Akula, Jihan Yang, Shusheng Yang, Adithya Iyer, Xichen Pan, et al. Cambrian-1: A fully open, vision-centric exploration of multimodal llms. *arXiv preprint arXiv:2406.16860*, 2024. 2, 3, 7
- [57] Wouter Van Gansbeke, Simon Vandenhende, and Luc Van Gool. Discovering object masks with transformers for unsupervised semantic segmentation. *arXiv preprint arXiv:2206.06363*, 2022. 4

- [58] Grant Van Horn, Elijah Cole, Sara Beery, Kimberly Wilber, Serge Belongie, and Oisín Mac Aodha. Benchmarking representation learning for natural world image collections. In *Proceedings of the IEEE/CVF conference on computer vision and pattern recognition*, pages 12884–12893, 2021. [2](#)
- [59] Xinlong Wang, Rufeng Zhang, Chunhua Shen, Tao Kong, and Lei Li. Dense contrastive learning for self-supervised visual pre-training. In *CVPR*, 2021. [4](#), [6](#), [2](#), [8](#), [9](#), [10](#)
- [60] Xinlong Wang, Zhiding Yu, Shalini De Mello, Jan Kautz, Anima Anandkumar, Chunhua Shen, and Jose M Alvarez. Freesolo: Learning to segment objects without annotations. In *Proceedings of the IEEE/CVF conference on computer vision and pattern recognition*, pages 14176–14186, 2022. [4](#)
- [61] Xudong Wang, Rohit Girdhar, Stella X. Yu, and Ishan Misra. Cut and learn for unsupervised object detection and instance segmentation, 2023. [4](#)
- [62] Chen Wei, Haoqi Fan, Saining Xie, Chao-Yuan Wu, Alan Yuille, and Christoph Feichtenhofer. Masked feature prediction for self-supervised visual pre-training. In *CVPR*, 2022. [2](#), [4](#), [6](#), [7](#), [8](#), [3](#), [9](#), [10](#)
- [63] Philippe Weinzaepfel, Vincent Leroy, Thomas Lucas, Romain Brégier, Yohann Cabon, Vaibhav Arora, Leonid Antsfeld, Boris Chidlovskii, Gabriela Csurka, and Jérôme Revaud. Croco: Self-supervised pre-training for 3d vision tasks by cross-view completion. *NeurIPS*, 35, 2022. [2](#)
- [64] Philippe Weinzaepfel, Thomas Lucas, Vincent Leroy, Yohann Cabon, Vaibhav Arora, Romain Brégier, Gabriela Csurka, Leonid Antsfeld, Boris Chidlovskii, and Jérôme Revaud. CroCo v2: Improved Cross-view Completion Pre-training for Stereo Matching and Optical Flow. In *ICCV*, 2023. [2](#)
- [65] Weinzaepfel, Philippe and Leroy, Vincent and Lucas, Thomas and Brégier, Romain and Cabon, Yohann and Arora, Vaibhav and Antsfeld, Leonid and Chidlovskii, Boris and Csurka, Gabriela and Revaud Jérôme. CroCo: Self-Supervised Pre-training for 3D Vision Tasks by Cross-View Completion. In *NeurIPS*, 2022. [8](#)
- [66] Zhirong Wu, Yuanjun Xiong, Stella Yu, and Dahua Lin. Un-supervised feature learning via non-parametric instance discrimination. In *CVPR*, 2018. [1](#), [2](#), [4](#), [8](#), [9](#), [10](#)
- [67] Xueting Yan, Ishan Misra, Abhinav Gupta, Deepti Ghadyaram, and Dhruv Mahajan. Clusterfit: Improving generalization of visual representations, 2019. [4](#), [1](#), [2](#), [8](#), [9](#), [10](#)
- [68] Amir R. Zamir, Alexander Sax, William B. Shen, Leonidas J. Guibas, Jitendra Malik, and Silvio Savarese. Taskonomy: Disentangling task transfer learning. In *CVPR*, 2018. [3](#)
- [69] Jure Zbontar, Li Jing, Ishan Misra, Yann LeCun, and Stéphane Deny. Barlow twins: Self-supervised learning via redundancy reduction, 2021. [2](#), [4](#), [6](#), [3](#), [8](#), [9](#), [10](#)
- [70] Richard Zhang, Phillip Isola, and Alexei A Efros. Colorful image colorization. In *ECCV*, 2016. [2](#)
- [71] Jinghao Zhou, Chen Wei, Huiyu Wang, Wei Shen, Cihang Xie, Alan Yuille, and Tao Kong. ibot: Image bert pre-training with online tokenizer. *arXiv preprint arXiv:2111.07832*, 2021. [1](#), [4](#), [6](#), [7](#), [8](#), [2](#), [9](#), [10](#)

# Probing the Mid-level Vision Capabilities of Self-Supervised Learning

## Supplementary Material

Sec. A provides an overview the self-supervised learning models (Tab. 5) included in our study. Sec. B details the evaluation metrics and presents the quantitative results (Tab. 6 - 11) for each mid-level vision task. Sec. C shows cases qualitative visualizations (Fig. 7 - 8).

### A. Self-supervised Learning Models

In our experiments, we select 22 SSL models from a wide range of categories based on two criteria: (1) coverage of the main approaches used for large-scale self-supervised training and (2) comparable model architecture and training data to allow fair comparisons. We primarily evaluate the publicly-available checkpoints pretrained on ImageNet1K [12] — the links to each checkpoint are included in Tab. 5. We briefly describe each SSL below.

**Jigsaw.** Noroozi and Favaro [46] introduced a self-supervised learning approach for model pretraining based on solving jigsaw puzzles as a pretext task. This method trains a network to predict the correct arrangement of shuffled image patches, where the image is divided into a 3x3 grid. At its core, this approach encourages the model to learn spatial relationships and understand object structure by generating consistent embeddings for the spatially rearranged patches of the same image. In our study, we used the publicly available ResNet-50 checkpoint trained on the ImageNet-1k [54] dataset.

**Rotnet.** Gidaris *et al.* [25] proposed a self-supervised approach for model pretraining using a rotation prediction task, known as RotNet. This method trains a network to classify the rotation angle (0°, 90°, 180°, or 270°) applied to an input image, encouraging the model to learn semantic features and spatial structure within the image. At its core, this approach leverages rotation as a proxy task, pushing the network to recognize objects and their orientations. In our work, we evaluate the ResNet-50 architecture trained on ImageNet-1k [54] using this pretext task and rely on the checkpoint released by the authors.

**NPID.** Wu *et al.* [66] introduced a non-parametric instance-level discrimination approach for unsupervised feature learning. This method trains a network to distinguish between individual instances by treating each image as its own unique class, employing a memory bank to store and update embeddings for all instances in the dataset. At its core, this approach promotes the model to learn discriminative features by maximizing the similarity between aug-

mentations of the same instance and minimizing it across others. In our work, we evaluate the ResNet-50 architecture pre-trained on ImageNet-1k [54] using this instance discrimination task.

**NPID++.** Misra *et al.* [43] significantly improves upon the original implementation of NPID, achieving results that substantially outperform those reported in the original paper [66].

**PIRL.** Misra *et al.* [43] introduced Self-Supervised Learning of Pretext-Invariant Representations (PIRL), a method designed to learn representations that remain invariant across various pretext tasks. The approach applies contrastive learning, where the model is trained to produce similar embeddings for multiple augmentations of the same image while distinguishing between different images. At its core, PIRL combines instance discrimination with pretext invariance to capture both semantic and structural features. In our work, we evaluate the ResNet-50 architecture pre-trained on ImageNet using the PIRL framework.

**ClusterFit.** Yan *et al.* [67] proposed ClusterFit, a self-supervised learning approach that improves feature representations through clustering and re-training. This method begins by clustering embeddings of unlabeled images to capture the underlying data distribution, using these cluster assignments as pseudo-labels to retrain the model, thus distilling semantic information at the cluster level. At its core, ClusterFit follows a two-step process—clustering followed by supervised re-training—to develop robust and discriminative features. In our work, we evaluate the checkpoint using ResNet-50 architecture which is pre-trained on ImageNet.

**SimCLR.** Chen *et al.* [6] proposed SimCLR, a contrastive self-supervised learning framework designed to learn visual representations by maximizing agreement between different augmented views of the same image. The method applies a series of data augmentations, including random cropping, color distortion, and Gaussian blur, and uses a contrastive loss to bring embeddings of the same image instance closer together while pushing apart embeddings of different images. At its core, SimCLR leverages a simple yet effective contrastive objective, removing the need for specialized architectures or memory banks. In our work, we evaluate the ResNet-50 architecture trained on ImageNet-1k [54].



Table 5. **Self-Supervised Model Details.** This table provides details about each model, including the backbone architecture, the dataset used for training, and the source links to the checkpoints utilized in our experiments.

Model Name	Backbone	Dataset	Source Link
Jigsaw [46]	ResNet-50	ImageNet-1K	<a href="#">VISSL model zoo</a>
RotNet [25]	ResNet-50	ImageNet-1K	<a href="#">VISSL model zoo</a>
NPID [66]	ResNet-50	ImageNet-1K	<a href="#">VISSL model zoo</a>
SeLa-v2 [4]	ResNet-50	ImageNet-1K	<a href="#">SwAV repository</a>
NPID++ [43]	ResNet-50	ImageNet-1K	<a href="#">VISSL model zoo</a>
PIRL [43]	ResNet-50	ImageNet-1K	<a href="#">VISSL model zoo</a>
ClusterFit [67]	ResNet-50	ImageNet-1K	<a href="#">VISSL model zoo</a>
DeepCluster-v2 [4]	ResNet-50	ImageNet-1K	<a href="#">SwAV repository</a>
SwAV [4]	ResNet-50	ImageNet-1K	<a href="#">SwAV repository</a>
SimCLR [6]	ResNet-50	ImageNet-1K	<a href="#">VISSL model zoo</a>
MoCo v2 [8]	ResNet-50	ImageNet-1K	<a href="#">MoCo v2 repository</a>
SimSiam [7]	ResNet-50	ImageNet-1K	<a href="#">MMSelfSup model zoo</a>
BYOL [28]	ResNet-50	ImageNet-1K	<a href="#">Unofficial BYOL repo</a>
Barlow Twins [69]	ResNet-50	ImageNet-1K	<a href="#">MMSelfSup model zoo</a>
DenseCL [59]	ResNet-50	ImageNet-1K	<a href="#">DenseCL repository</a>
DINO [5]	ResNet-50/ViT-B/16	ImageNet-1K	<a href="#">DINO repository</a>
MoCo v3 [9]	ResNet-50/ViT-B/16	ImageNet-1K	<a href="#">MoCo v3 repository</a>
iBOT [71]	ViT-B/16	ImageNet-1K	<a href="#">iBOT repository</a>
MAE [31]	ViT-B/16	ImageNet-1K	<a href="#">MAE repository</a>
MaskFeat [62]	ViT-B/16	ImageNet-1K	<a href="#">MMSelfSup model zoo</a>

**SwAV.** Caron *et al.* [4] introduced SwAV (Swapping Assignments between Views), a self-supervised learning approach that combines clustering with contrastive learning. Instead of directly contrasting augmented views, SwAV clusters the features of one view and assigns pseudo-labels, which are then used to predict the cluster assignments of another view. This method enables the model to learn representations without requiring negative samples or a memory bank. At its core, SwAV maximizes similarity between different augmentations by leveraging these swapped cluster assignments. In our work, we evaluate the ResNet-50 architecture trained on ImageNet 1k with SwAV.

**SeLa-v2.** SeLa [1] proposes an alternative approach to clustering-based self-supervised learning by formulating the clustering process as an optimization problem. It uses the Sinkhorn-Knopp algorithm to solve this optimization efficiently, ensuring that cluster assignments are balanced across the dataset. This avoids degenerate solutions where all data points are assigned to a single cluster. Caron *et al.* [4] re-implemented SeLa which improves upon the original SeLa by incorporating additional training improvements introduced in the self-supervised learning literature, such as stronger data augmentation, an MLP projection head, and temperature scaling for contrastive learning and yields better performance.

**MoCo-v2.** Chen *et al.* [8] proposed MoCo-v2, an improved version of the Momentum Contrast (MoCo) framework for self-supervised learning. MoCo-v2 enhances the original MoCo by incorporating stronger data augmenta-

tions (such as color distortion and Gaussian blur) and using an MLP projection head to further improve representation quality. Similar to its predecessor, MoCo-v2 employs a memory bank to maintain a large pool of negative samples and uses a momentum-updated encoder to produce stable representations. At its core, this approach refines instance discrimination with updated augmentations and architecture adjustments. In our work, we evaluate the ResNet-50 architecture trained on ImageNet using MoCo-v2.

**SimSiam.** Chen and He [7] proposed SimSiam, a self-supervised learning framework designed to simplify contrastive learning by removing the need for negative samples, momentum encoders, or memory banks. Instead, SimSiam trains a Siamese network with two branches, where one branch predicts the representation of the other. By using only a stop-gradient operation on one branch, SimSiam prevents the network from collapsing to trivial solutions, allowing it to learn meaningful representations from positive pairs alone. At its core, SimSiam is a simple and efficient method that demonstrates the feasibility of contrastive learning without negatives. In our work, we evaluate the ResNet-50 architecture trained on ImageNet 1k with SimSiam.

**DenseCL.** Wang *et al.* [59] introduced DenseCL, a self-supervised learning approach that extends contrastive learning to dense feature correspondences within images. Unlike traditional contrastive methods focused on global representations, DenseCL aims to learn pixel-level features by contrasting dense local regions between augmented views

of the same image. This pixel-level contrastive objective encourages the model to learn spatially detailed representations, which benefit dense prediction tasks such as object detection and segmentation. At its core, DenseCL leverages fine-grained contrastive learning to produce more spatially aware features. In our work, we evaluate the ResNet-50 architecture trained on ImageNet 1k using DenseCL.

**BYOL.** Grill *et al.* [28] proposed BYOL, a self-supervised learning framework that learns visual representations without requiring negative samples. BYOL employs two neural networks: a “student” network and a “target” network. The student learns to predict the target’s representation of an augmented view of the same image, and the target network is updated as an exponential moving average of the student. This setup enables the model to avoid trivial solutions by progressively refining representations through self-distillation. At its core, BYOL relies on bootstrap mechanisms and a momentum update to learn meaningful features without contrastive pairs. In our work, we evaluate the ResNet-50 architecture trained on ImageNet 1k using BYOL.

**DeepCluster-v2.** Caron *et al.* [3] introduced DeepCluster which uses k-means clustering on deep features to assign pseudo-labels to unlabeled data. These pseudo-labels are then used for training the network in an iterative process. However, DeepCluster suffers from the instability of cluster assignments between epochs, which requires reinitializing the classification layer repeatedly, disrupting the training of the convolutional network. Caron *et al.* [4] reimplement DeepCluster and address earlier issues by introducing explicit comparisons between features and cluster centroids instead of learning a classification layer for cluster assignments. This direct comparison increases the stability and performance of the training process. Additionally, DeepCluster-v2 incorporates modern self-supervised learning tricks and further enhances the method’s performances.

**Barlow Twins.** Zbontar *et al.* [69] proposed Barlow Twins, a self-supervised learning approach designed to reduce redundancy in representations by decorrelating feature dimensions. The method uses a loss function that encourages the cross-correlation matrix between two identical networks’ embeddings of augmented views to be as close to the identity matrix as possible, reducing redundancy across dimensions. This setup allows the model to learn diverse and informative features without the need for negative samples or memory banks. At its core, Barlow Twins promotes redundancy reduction, enhancing feature decorrelation. In our work, we evaluate the ResNet-50 architecture pre-trained on ImageNet 1k using Barlow Twins.

**MoCo-v3.** Chen *et al.* [9] proposed MoCo-v3, an extension of the Momentum Contrast framework tailored for Vision Transformers (ViTs) in self-supervised learning. MoCo-v3 adapts the momentum contrastive learning strategy to ViTs, introducing optimizations such as an MLP projection head and advanced data augmentations. Similar to previous versions, MoCo-v3 leverages a momentum-updated encoder to generate stable features and uses a queue-based memory bank to manage negative samples. At its core, this approach refines contrastive learning by combining MoCo’s momentum mechanism with the ViT architecture. In our work, we evaluate the ViT-B/16 architecture trained on ImageNet using MoCo-v3 and employ the checkpoint released by the authors.

**DINO.** Caron *et al.* [5] proposed a self-distillation approach for model pretraining. The proposed approach trains a student network to generate features similar to a teacher network, where the teacher is an exponential moving average of the student network. At its core, this approach relies on instance discrimination as the model is trained to learn to generate similar embeddings for different crops of the same image instance. In our work, we evaluate the ViT-B/16 architecture trained on ImageNet-1k. We use the checkpoint released by the authors.

**MAE.** He *et al.* [31] showed that training vision transformers to reconstruct images based on randomly masked inputs is an effective pretraining task. Such models are trained with a large masking ratio; e.g., 75% of the input image patches are masked. In our experiments, we use the ViT-B/16 and ViT-L/16 models trained on ImageNet-1k.

**MaskFeat.** Wei *et al.* [62] introduced MaskFeat, a self-supervised learning approach that learns visual representations by predicting masked visual tokens in videos. MaskFeat leverages a Vision Transformer (ViT) and operates by masking random patches in input video frames, then training the model to predict feature embeddings of these masked regions. This strategy encourages the model to capture rich semantic and spatial features, which generalize well across various downstream tasks. At its core, MaskFeat combines masked prediction with a ViT backbone, making it particularly effective for dense prediction tasks. In our work, we evaluate the ViT-B/16 architecture trained on ImageNet-1k using MaskFeat.

**BEiT-v2.** Peng *et al.* [49] proposed BEiT-v2, a self-supervised learning method that improves upon the original BEiT by introducing a more refined tokenization process for masked image modeling. BEiT-v2 leverages a teacher-student framework, where the teacher network generates

discrete tokens from image patches, and the student network learns to predict these tokens from masked image patches. This approach enhances the model’s ability to capture fine-grained visual patterns and contextual relationships. At its core, BEiT-v2 combines masked image modeling with a new tokenization strategy to achieve state-of-the-art performance on image classification and downstream tasks. In our work, we evaluate the ViT-B/16 architecture trained on ImageNet-1k using BEiT-v2.

**iBOT.** Zhou *et al.* [71] combine ideas from DINO and MAE by training a model to reconstruct masked dense features based on a teacher network. iBOT uses both an image-level and a dense distillation objective. We analyze the ViT-B/16 and ViT-L/16 architectures trained on ImageNet1k and ImageNet-22k. We evaluate the checkpoints released by the authors.

## B. Task-Specific Metric Descriptions

**Generic Object Segmentation** We report the full results in Tab. 6 using the following metrics to evaluate generic object segmentation, which involves binary segmentation of foreground objects and background:

- **F1 Score:** The F1 score provides a harmonic mean of precision and recall, offering a balanced evaluation of segmentation performance, particularly in the presence of class imbalance. It is defined as:

$$F1 = \frac{2 \cdot \text{Precision} \cdot \text{Recall}}{\text{Precision} + \text{Recall}}$$

where **Precision** measures the proportion of correctly predicted foreground pixels among all pixels predicted as foreground, and **Recall** measures the proportion of correctly predicted foreground pixels relative to all ground truth foreground pixels.

- **Accuracy:** Accuracy quantifies the proportion of correctly classified pixels, encompassing both foreground and background classes. It is defined as:

$$\text{Accuracy} = \frac{\text{Correct Predictions} \cdot (\text{Fore.} + \text{Back.})}{\text{Total Pixels}}$$

While simple and intuitive, accuracy may be biased toward the majority class (e.g., background), particularly in cases of class imbalance.

- **Mean Intersection over Union (mIoU):** mIoU assesses segmentation performance by averaging the Intersection over Union (IoU) across all classes (foreground and background). For a given class  $c$ , IoU is defined as:

$$\text{IoU}_c = \frac{\text{TP}_c}{\text{TP}_c + \text{FP}_c + \text{FN}_c}$$

where  $\text{TP}_c$ ,  $\text{FP}_c$ , and  $\text{FN}_c$  denote the true positives, false positives, and false negatives for class  $c$ . mIoU is computed as:

$$\text{mIoU} = \frac{1}{C} \sum_{c=1}^C \text{IoU}_c$$

where  $C = 2$  for generic object segmentation. mIoU provides a robust evaluation of the model’s capacity to capture spatial overlap and resolve fine-grained boundaries.

These metrics collectively provide a comprehensive evaluation of the model’s performance in binary segmentation tasks, highlighting both pixel-level accuracy and the model’s ability to distinguish between foreground and background regions.

**Depth Prediction** We present the complete results for depth prediction in Tab. 7. To evaluate performance, we adopt the setup described in [16], which includes computing the root mean square error (RMSE) and evaluating the prediction accuracy under different threshold criteria. The threshold-based accuracy, denoted as  $\delta_i$ , measures the proportion of pixels for which the ratio between the predicted depth ( $d^{pr}$ ) and the ground-truth depth ( $d^{gt}$ ) lies below  $1.25^i$ . Formally, this is defined as:

$$\delta_i(d^{pr}, d^{gt}) = \frac{1}{N} \sum_{j=1}^N \left[ \max \left( \frac{d_j^{pr}}{d_j^{gt}}, \frac{d_j^{gt}}{d_j^{pr}} \right) < 1.25^i \right] \quad (1)$$

where  $N$  is the total number of pixels,  $d^{pr}$  represents the predicted depth, and  $d^{gt}$  is the ground-truth depth.

**Surface Normal Estimation** For each pixel in the image, the error is defined as the angular deviation (in degrees) between the predicted and ground-truth surface normals. To evaluate the model’s performance, we compute two primary metrics: (1) the root mean square error (RMSE), which measures the overall angular error, and (2) the accuracy of predictions at predefined angular thresholds. Specifically, the accuracy metric is calculated as the proportion of pixels whose angular error falls within thresholds of  $11.25^\circ$ ,  $22.5^\circ$ , and  $30^\circ$ , following established evaluation protocols [2, 22, 50].

**Geometric Correspondence** We report full results on object geometric correspondence in Tab. 9 and scene geometric correspondence in Tab. 10. Correspondences are evaluated using either 2D projection error or 3D metric error. For a correspondence between pixel locations  $p$  in image 1 and  $q$  in image 2, the 2D projection error is computed as follows. First,  $p$  is projected into 3D space, yielding a 3D point  $\mathbf{P}$ , using the depth value at  $p$  and the camera intrinsics of image 1. The 3D point  $\mathbf{P}$  is transformed to the coordinate frame of

image 2 using the relative camera pose and projected back onto the image plane of image 2, yielding the pixel location  $p'$ . The 2D projection error is then defined as:

$$\text{Error}_{2D} = \|p' - q\|_2$$

where  $\|\cdot\|_2$  represents the Euclidean distance in the image plane.

For 3D metric error, both  $p$  and  $q$  are transformed into a shared 3D coordinate space, resulting in  $\mathbf{P}$  and  $\mathbf{Q}$ , respectively. The 3D metric error is then computed as:

$$\text{Error}_{3D} = \|\mathbf{P} - \mathbf{Q}\|_2$$

The 2D projection error is used for scene-level correspondences, while the 3D metric error is preferred for objects to better account for occlusions and thin structures.

To evaluate correspondence quality, we compute *correspondence recall*, defined as the percentage of correspondences with error below a threshold  $\tau$ :

$$\text{Recall} = \frac{|\{\text{Error} < \tau\}|}{N}$$

Where  $|\{\text{Error} < \tau\}|$  indicates the number of correspondences with error below the threshold  $\tau$  and  $N$  is the total number of correspondences. We report recall values for various  $\tau$  values and analyze results across image pairs grouped by relative viewpoint changes.

**Mid-level Image Similarity** We present the full results for mid-level image similarity in Tab. 11. In this task, a reference image is provided, and the model selects one of two candidate images based on mid-level image similarity. The evaluation metrics used are Accuracy (Acc), Precision (Prec), Recall (Rec), and F1 Score (F1), defined as follows: **Accuracy (Acc):** The proportion of correctly predicted matches out of the total comparisons:

$$\text{Acc} = \frac{\text{Correct Predictions}}{\text{Total Comparisons}}$$

**Precision (Prec):** The proportion of correctly identified matches (true positives, TP) among all images predicted as matches:

$$\text{Prec} = \frac{\text{TP}}{\text{TP} + \text{False Positives (FP)}}$$

**Recall (Rec):** The proportion of correctly identified matches (TP) among all actual matches in the dataset:

$$\text{Rec} = \frac{\text{TP}}{\text{TP} + \text{False Negatives (FN)}}$$

**F1 Score (F1):** The harmonic mean of Precision and Recall, providing a balanced measure of performance:

$$\text{F1} = \frac{2 \cdot \text{Prec} \cdot \text{Rec}}{\text{Prec} + \text{Rec}}$$

These metrics provide a rigorous evaluation of the model’s ability to identify mid-level image similarities accurately and consistently.

## C. Qualitative Comparisons

We present qualitative visualizations in Fig. 7 and Fig. 8 to assess model performance on mid-level vision tasks. These visualizations validate the models’ ability to learn and perform each mid level vision task effectively.



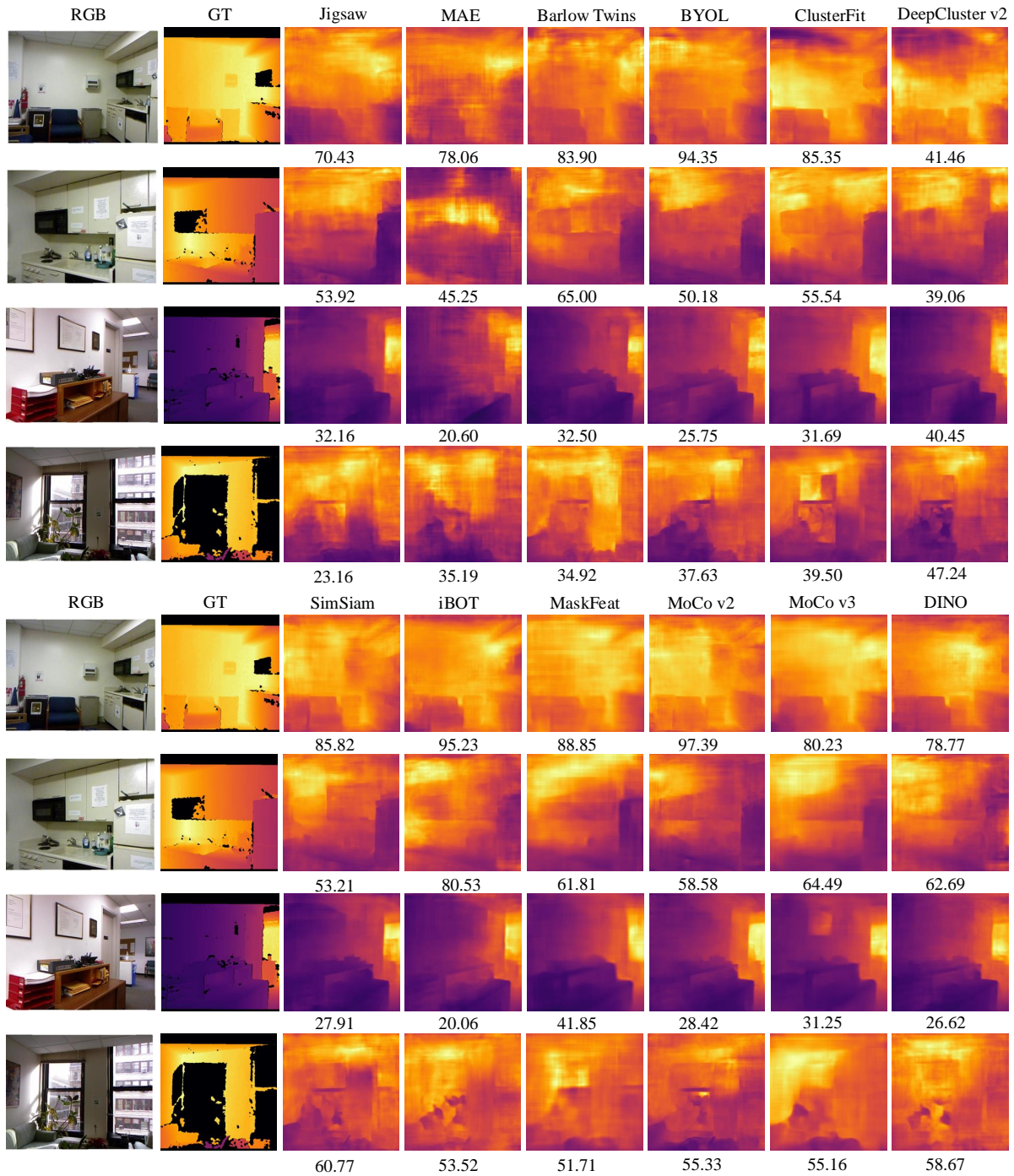


Figure 7. **Qualitative Depth Estimation Results for Selected SSL Models.** Depth estimation visualizations are shown for selected SSL models, with the  $\delta_1$  score displayed below each visualization (*higher is better*). These results highlight the models’ effectiveness in capturing depth information. Note DINO and MoCo v3 are ViT based.

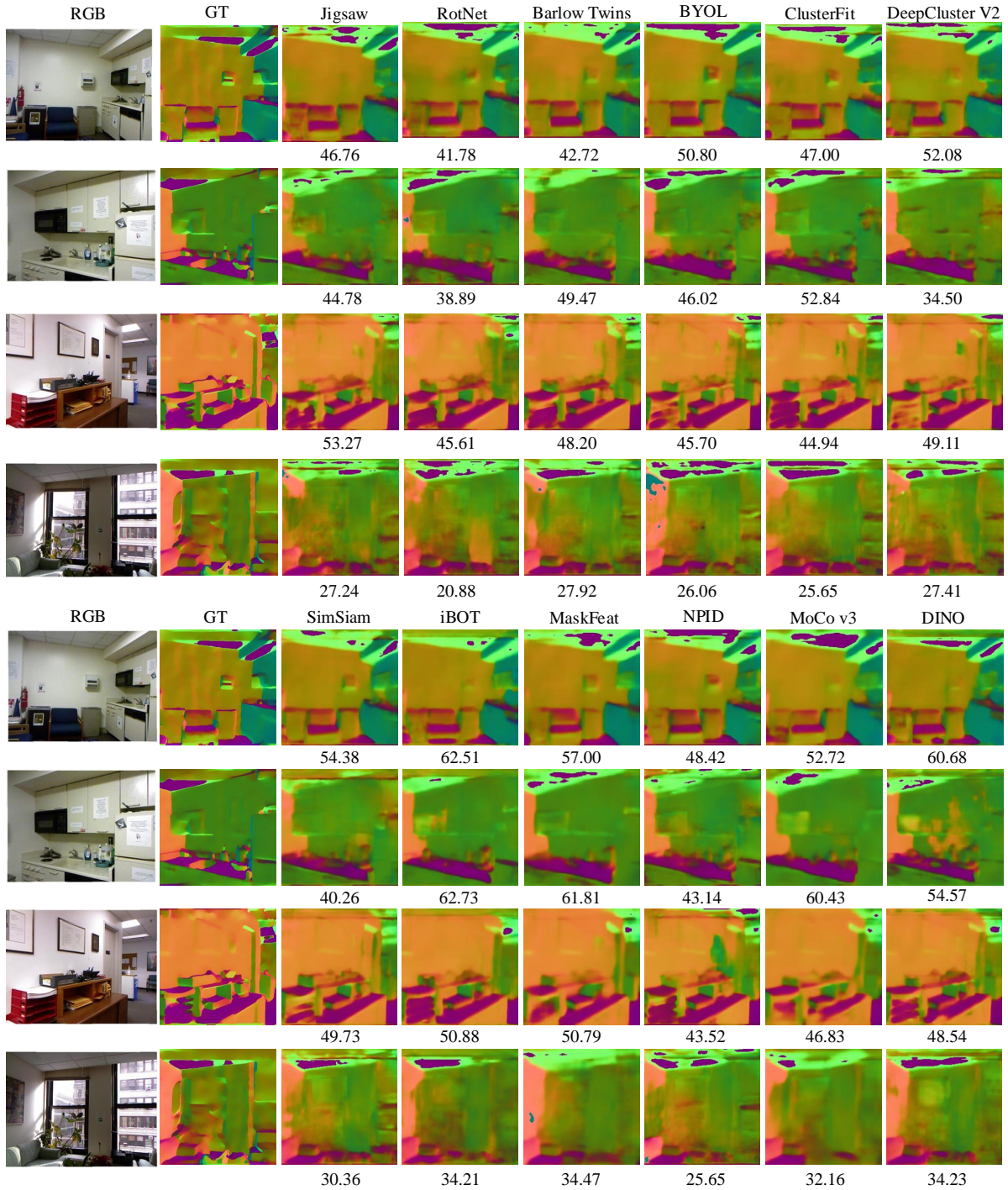


Figure 8. **Qualitative Surface Normal Estimation Results for Selected SSL Models.** Surface normal estimation visualizations are shown for selected SSL models, with the  $\delta_1$  score displayed below each visualization (*higher is better*). These results highlight the models' effectiveness in capturing surface normal information. Note DINO and MoCo v3 are ViT based.

Table 6. **2D Grouping Results (Generic Object Segmentation).** Evaluation results for generic object segmentation, where models segment foreground objects from the background, are presented for both VOC07 [19] and VOC12 [20] datasets.

Model	Backbone	Task	VOC07 [19]			VOC12 [20]		
			F1-measure	mIoU	Accuracy	F1-measure	mIoU	Accuracy
<i>Self-Supervised Models (SSL)</i>								
Jigsaw [46]	RN-50	IN-1k	71.13	63.03	83.24	81.51	71.48	89.41
RotNet [25]	RN-50	IN-1k	75.84	65.32	85.39	83.46	71.46	89.94
NPID [66]	RN-50	IN-1k	76.92	66.38	85.99	84.34	72.66	90.35
SeLa-v2 [4]	RN-50	IN-1k	83.20	73.53	89.73	86.03	76.56	91.71
NPID++ [43]	RN-50	IN-1k	80.75	69.59	87.84	85.46	75.24	91.29
PIRL [43]	RN-50	IN-1k	79.55	69.62	87.69	86.40	77.39	92.46
ClusterFit [67]	RN-50	IN-1k	77.91	67.94	86.79	85.58	72.98	90.25
DeepCluster-v2 [4]	RN-50	IN-1k	79.33	71.08	88.14	88.29	79.91	93.01
SwAV [4]	RN-50	IN-1k	79.72	71.95	88.59	87.38	78.72	92.91
SimCLR [6]	RN-50	IN-1k	81.05	73.63	89.44	87.94	79.62	93.25
MoCo v2 [8]	RN-50	IN-1k	82.78	74.40	89.91	88.65	79.75	93.21
SimSiam [7]	RN-50	IN-1k	82.99	74.05	89.88	88.25	77.51	92.05
BYOL [28]	RN-50	IN-1k	83.20	71.97	89.21	87.74	78.81	93.09
Barlow Twins [69]	RN-50	IN-1k	79.97	71.53	88.51	88.09	78.62	92.82
DenseCL [59]	RN-50	IN-1k	79.32	70.71	88.03	87.19	78.75	92.47
DINO [5]	RN-50	IN-1k	78.13	71.95	88.32	88.81	79.86	92.99
MoCo v3 [9]	RN-50	IN-1k	82.56	71.48	88.88	85.44	77.41	92.06
DINO [5]	ViT-B/16	IN-1k	83.12	74.00	89.79	88.70	79.94	93.17
iBOT [71]	ViT-B/16	IN-1k	82.85	75.74	90.50	90.51	84.72	94.90
MoCo v3 [9]	ViT-B/16	IN-1k	80.92	72.45	88.99	82.11	74.11	90.71
MAE [31]	ViT-B/16	IN-1k	77.25	65.78	85.88	80.22	69.63	89.14
MaskFeat [62]	ViT-B/16	IN-1k	78.84	70.28	87.76	84.27	75.14	91.00

Table 7. **Depth Estimation Results for SSL Models on NYU and NAVI.** Results for scene-level (NYU) and object-level (NAVI) depth estimation using self-supervised models. These results demonstrate the performance of SSL models across diverse depth estimation tasks.

Model	Architecture	Dataset	NYU				NAVI			
			$\delta_1$	$\delta_2$	$\delta_3$	RMSE	$\delta_1$	$\delta_2$	$\delta_3$	RMSE
<i>Self-Supervised Models</i>										
Jigsaw [46]	RN-50	IN-1k	71.17	93.02	98.24	0.6282	29.48	55.45	73.66	0.1775
RotNet [25]	RN-50	IN-1k	73.18	93.41	98.23	0.6047	29.87	55.03	73.00	0.1804
NPID [66]	RN-50	IN-1k	70.65	92.81	98.34	0.6191	37.88	65.46	80.82	0.1506
Sela-v2 [4]	RN-50	IN-1k	74.76	94.47	98.80	0.5684	34.72	61.97	78.64	0.1586
NPID++ [43]	RN-50	IN-1k	71.89	93.27	98.34	0.6110	38.07	65.32	80.69	0.1525
PIRL [43]	RN-50	IN-1k	74.58	94.13	98.59	0.5780	38.55	65.36	80.86	0.1495
ClusterFit [67]	RN-50	IN-1k	74.13	93.81	98.25	0.5850	39.45	66.47	81.45	0.1479
DeepCluster-v2 [4]	RN-50	IN-1k	73.63	93.62	98.39	0.5863	39.50	67.35	82.43	0.1448
SwAV [4]	RN-50	IN-1k	76.17	94.96	98.81	0.5542	39.45	67.13	82.04	0.1457
SimCLR [6]	RN-50	IN-1k	75.64	94.67	98.65	0.5698	42.86	70.04	83.68	0.1365
MoCo v2 [8]	RN-50	IN-1k	77.05	94.83	98.77	0.5467	45.42	72.55	85.42	0.1309
SimSiam [7]	RN-50	IN-1k	75.95	94.74	98.78	0.5628	43.03	70.01	83.94	0.1366
BYOL [28]	RN-50	IN-1k	75.43	94.48	98.68	0.5711	42.19	69.22	83.54	0.1387
Barlow Twins [69]	RN-50	IN-1k	75.06	94.22	98.61	0.5791	41.83	68.74	83.01	0.1408
DenseCL [59]	RN-50	IN-1k	76.30	94.69	98.65	0.5615	43.78	71.45	85.01	0.1332
DINO [5]	RN-50	IN-1k	77.68	95.89	99.09	0.5235	47.63	74.31	86.54	0.1241
MoCo v3 [9]	RN-50	IN-1k	75.56	94.63	98.86	0.5584	45.93	72.87	85.57	0.1309
DINO [5]	ViT-B/16	IN-1k	79.38	95.97	99.05	0.5278	47.75	74.65	87.02	0.1241
iBOT [71]	ViT-B/16	IN-1k	81.32	96.90	99.34	0.4919	50.02	76.29	87.89	0.1199
MoCo v3 [9]	ViT-B/16	IN-1k	80.14	96.14	99.16	0.5109	51.07	76.96	87.95	0.1175
MAE [31]	ViT-B/16	IN-1k	66.17	90.38	97.37	0.6898	26.78	51.82	71.69	0.1868
MaskFeat [62]	ViT-B/16	IN-1k	80.39	96.18	99.07	0.5125	49.50	75.47	87.14	0.1195



Table 8. **Surface Normal Estimation Results on NYUv2 and NAVI Datasets.** Performance of self-supervised models on scene-level (NYUv2) and object-level (NAVI) surface normal estimation, evaluated using angular thresholds (11.25°, 22.5°, 30°) and RMSE metrics.

Model	Backbone	Dataset	NYUv2				NAVI			
			11.25°	22.5°	30°	RMSE	11.25°	22.5°	30°	RMSE
<i>Self-Supervised Models</i>										
Jigsaw [46]	RN-50	IN-1k	44.27	67.65	76.23	28.8386	22.79	49.22	62.50	36.6169
RotNet [25]	RN-50	IN-1k	43.93	67.40	76.07	28.8557	23.70	50.20	63.46	28.8557
NPID [66]	RN-50	IN-1k	40.80	64.68	73.97	35.4511	24.92	51.82	64.87	35.4511
SeLa-v2 [4]	RN-50	IN-1k	45.14	68.98	77.53	28.0449	25.73	53.19	66.22	34.7204
NPID++ [43]	RN-50	IN-1k	41.57	65.98	75.14	29.2829	25.03	52.03	65.20	34.9940
PIRL [43]	RN-50	IN-1k	44.92	68.35	76.71	28.5771	27.01	54.06	66.85	34.1514
ClusterFit [67]	RN-50	IN-1k	43.93	67.40	76.12	28.9261	25.49	53.21	65.98	34.8134
Deepcluster-v2 [4]	RN-50	IN-1k	44.48	68.29	76.98	28.2509	26.51	54.01	67.07	34.1514
SwAV [4]	RN-50	IN-1k	44.08	67.98	76.81	28.2881	25.69	53.17	66.21	34.4863
SimCLR [6]	RN-50	IN-1k	45.87	69.17	77.48	27.9438	26.70	54.21	67.07	34.1743
MoCo v2 [8]	RN-50	IN-1k	46.37	69.79	78.03	27.5874	29.02	56.86	69.42	32.7033
SimSiam [7]	RN-50	IN-1k	44.12	67.95	76.72	28.4032	28.06	55.71	68.18	33.5474
BYOL [28]	RN-50	IN-1k	43.64	67.73	76.46	28.5432	26.51	54.29	67.17	34.1015
Barlow Twins [69]	RN-50	IN-1k	44.04	67.75	76.57	28.4161	27.21	54.70	67.46	33.9390
DenseCL [59]	RN-50	IN-1k	45.30	68.74	77.16	28.2974	27.21	54.70	67.46	33.9390
DINO [5]	RN-50	IN-1k	47.64	70.96	79.12	26.8891	31.43	59.50	71.77	31.3895
MoCo v3 [9]	RN-50	IN-1k	43.03	67.15	76.20	28.6994	27.22	55.03	67.85	33.7240
DINO [5]	ViT-B/16	IN-1k	48.42	69.71	77.57	28.0873	31.66	58.58	70.68	31.9912
iBOT [71]	ViT-B/16	IN-1k	52.02	72.43	79.53	26.9539	32.75	60.06	71.69	31.4563
MoCo v3 [9]	ViT-B/16	IN-1k	49.64	70.01	77.36	28.2596	31.72	57.84	69.20	33.0295
MAE [32]	ViT-B/16	IN-1k	43.89	66.13	74.56	30.1382	22.07	49.06	62.63	36.4724
MaskFeat [62]	ViT-B/16	IN-1k	53.63	72.23	79.03	27.1797	32.40	58.92	70.43	32.3430

Table 9. **Geometric Correspondence Results on the NAVI Dataset.** Evaluation of self-supervised models on geometric correspondence tasks, including 3D Recall, 2D Projection Recall, and Binned Recall, across varying viewpoint angle ranges.

Model	Architecture	Dataset	3D Recall			2D Recall			Bin Recall			
			0.01m	0.02m	0.05m	5px	25px	50px	0-30°	30-60°	60-90°	90-120°
<i>Self-Supervised Models (SSL)</i>												
Jigsaw [46]	RN-50	IN-1k	9.13	19.83	54.94	0.68	7.45	16.20	49.15	26.54	13.06	7.76
RotNet [25]	RN-50	IN-1k	11.97	23.21	55.13	0.92	9.83	19.38	58.44	29.82	14.85	10.26
NPID [66]	RN-50	IN-1k	18.70	32.11	63.38	1.57	15.80	27.47	69.09	41.51	22.96	16.62
SeLa v2 [4]	RN-50	IN-1k	12.17	23.50	53.26	0.93	10.14	19.49	49.33	28.07	18.86	12.86
NPID++ [43]	RN-50	IN-1k	13.20	25.86	58.25	0.87	10.52	21.20	53.10	32.17	19.75	14.41
PIRL [43]	RN-50	IN-1k	16.21	29.49	61.54	1.15	13.21	24.73	60.73	36.56	22.61	16.40
ClusterFit [67]	RN-50	IN-1k	10.85	21.49	56.86	1.86	9.08	16.94	43.28	26.57	17.32	11.61
DeepCluster v2 [4]	RN-50	IN-1k	20.65	34.42	64.24	1.78	18.14	30.46	69.52	42.24	27.47	19.09
SwAV [4]	RN-50	IN-1k	20.20	33.99	63.20	1.71	17.60	29.83	67.11	42.34	27.23	18.81
SimCLR [6]	RN-50	IN-1k	16.57	30.68	61.75	1.09	13.49	25.80	60.53	37.77	23.67	18.27
MoCo v2 [8]	RN-50	IN-1k	21.85	37.76	68.76	1.63	18.17	32.94	75.85	48.73	28.47	20.50
SimSiam [7]	RN-50	IN-1k	23.47	38.16	68.41	2.07	20.16	33.57	76.05	48.63	29.90	20.46
BYOL [28]	RN-50	IN-1k	10.81	21.11	56.81	2.26	9.02	16.64	46.24	26.45	15.82	10.65
Barlow Twins [69]	RN-50	IN-1k	12.71	23.27	58.22	2.97	10.92	18.83	52.25	29.38	17.00	11.41
DenseCL [59]	RN-50	IN-1k	17.59	34.57	67.63	1.17	14.28	29.17	71.25	44.65	26.29	17.76
DINO [5]	RN-50	NAVI	30.57	47.36	75.43	2.61	26.79	42.41	84.37	61.43	39.01	26.82
MoCo v3 [9]	RN-50	NAVI	21.70	36.29	65.49	1.70	18.43	31.77	73.41	45.90	27.84	19.88
DINO [5]	ViT-B/16	IN-1k	25.91	43.00	74.66	3.16	22.54	36.86	84.78	56.28	33.20	22.54
iBOT [71]	ViT-B/16	IN-1k	26.84	44.72	76.10	3.12	23.78	39.11	86.94	58.98	34.22	23.85
MoCo v3 [9]	ViT-B/16	IN-1k	26.99	44.46	75.22	2.17	23.45	39.54	85.95	58.96	34.45	23.20
MAE [31]	ViT-B/16	IN-1k	19.21	32.59	66.82	2.74	17.16	27.72	78.17	46.12	21.16	11.85
MaskFeat [62]	ViT-B/16	IN-1k	22.11	35.16	65.92	2.08	19.67	31.37	86.25	51.50	22.17	11.00



Table 10. **Geometric Correspondence Results on ScanNet.** Evaluation of self-supervised models on 2D Projection Recall at varying pixel error thresholds and Binned Recall across viewpoint angle ranges.

Model	Architecture	2D Recall			Bin Recall			
		5px	10px	20px	0-15°	15-30°	30-60°	60-180°
<i>Self-Supervised Models</i>								
Jigsaw [46]	RN-50	9.57	18.18	27.98	26.11	19.80	11.16	4.00
RotNet [25]	RN-50	15.74	25.46	34.15	37.56	28.52	13.73	4.29
NPID [66]	RN-50	27.64	40.10	50.07	52.84	44.85	28.24	11.34
SeLa-v2 [4]	RN-50	12.21	22.70	33.36	31.73	24.61	14.61	6.54
NPID++ [43]	RN-50	10.62	19.59	30.23	27.16	20.92	13.09	6.37
PIRL [43]	RN-50	17.89	30.43	41.35	45.37	35.12	19.67	7.55
ClusterFit [67]	RN-50	26.31	40.92	51.96	54.96	46.61	26.67	10.45
DeepCluster v2 [4]	RN-50	17.30	27.90	37.57	38.25	30.90	18.09	7.87
SwAV [4]	RN-50	25.41	38.74	49.86	52.34	44.20	27.48	10.23
SimCLR [6]	RN-50	21.78	35.34	46.18	48.85	40.32	22.15	9.08
MoCo v2 [8]	RN-50	24.92	37.65	48.33	50.92	41.97	24.56	8.97
SimSiam [7]	RN-50	18.11	29.83	40.92	42.58	33.72	19.04	7.24
BYOL [28]	RN-50	15.39	25.41	34.89	35.88	26.91	16.96	6.90
Barlow Twins [69]	RN-50	18.83	30.60	40.61	42.36	33.96	19.24	8.55
DenseCL [59]	RN-50	17.23	31.17	44.98	42.41	34.80	20.36	8.56
DINO [5]	RN-50	26.63	40.64	51.49	54.07	45.63	27.80	11.19
MoCo v3 [9]	RN-50	15.23	26.06	35.87	37.24	28.23	15.94	7.05
DINO [5]	ViT-B/16	24.38	34.22	45.47	46.56	36.72	23.74	11.12
iBOT [71]	ViT-B/16	20.04	29.45	41.07	41.13	30.95	20.00	9.47
MoCo v3 [9]	ViT-B/16	25.03	39.31	51.00	53.18	42.87	27.05	11.95
MAE [32]	ViT-B/16	6.64	10.31	18.42	15.64	9.81	6.63	3.81
MaskFeat [62]	ViT-B/16	27.94	40.87	50.49	56.51	47.65	24.41	6.90

Table 11. **Image Retrieval Results on the NIGHTS Dataset.** Retrieval performance is evaluated using Accuracy, F1-score, Precision, and Recall. Results are reported for self-supervised models using ResNet-50 and ViT-B/16 backbones, highlighting their capability to retrieve similar images based on mid-level features.

Model	Backbone	Dataset	Accuracy	F1-Score	Precision	Recall
<i>Self-Supervised Models (SSL)</i>						
Jigsaw [46]	RN-50	NIGHTS	71.22	70.69	70.73	70.65
RotNet [25]	RN-50	NIGHTS	75.33	75.14	74.40	75.89
NPID [66]	RN-50	NIGHTS	81.41	81.16	80.84	81.47
SeLa-v2 [4]	RN-50	NIGHTS	81.41	81.16	80.84	81.47
NPID++ [43]	RN-50	NIGHTS	83.06	82.63	83.24	82.03
PIRL [43]	RN-50	NIGHTS	83.77	83.56	83.19	83.93
ClusterFit [67]	RN-50	NIGHTS	81.58	81.42	80.70	82.14
DeepCluster-v2 [4]	RN-50	NIGHTS	85.25	84.93	85.26	84.60
SwAV [4]	RN-50	NIGHTS	84.65	84.36	84.45	84.26
SimCLR [6]	RN-50	NIGHTS	83.55	83.26	83.26	83.26
MoCo v2 [8]	RN-50	NIGHTS	84.43	84.22	83.85	84.60
SimSiam [7]	RN-50	NIGHTS	85.86	85.78	84.75	86.83
BYOL [28]	RN-50	NIGHTS	85.86	85.75	84.90	86.61
Barlow Twins [69]	RN-50	NIGHTS	83.11	82.70	83.26	82.14
DenseCL [59]	RN-50	NIGHTS	82.73	82.53	82.03	83.04
DINO [5]	RN-50	NIGHTS	83.83	83.31	84.50	82.14
MoCo v3 [9]	RN-50	NIGHTS	84.70	84.37	84.70	84.04
DINO [5]	ViT-B/16	NIGHTS	89.20	88.98	89.23	88.73
iBOT [71]	ViT-B/16	NIGHTS	89.36	89.27	88.49	90.07
MoCo v3 [9]	ViT-B/16	NIGHTS	87.17	86.90	87.19	86.61
MAE [31]	ViT-B/16	NIGHTS	83.39	82.91	83.81	82.03
MaskFeat [62]	ViT-B/16	NIGHTS	76.10	75.70	75.61	75.78